

Phenomenological $\pi N \rightarrow \pi\pi N$ Amplitude and Analysis of Low Energy Data on Total Cross Sections and 1-D Distributions

A.A. Bolokhov

Sankt-Petersburg State University, Sankt-Petersburg, 198904, Russia

M.V. Polyakov and S.G. Sherman

St. Petersburg Institute for Nuclear Physics, Sankt-Petersburg, 188350, Russia

Abstract

We develop the phenomenological amplitude of the $\pi N \rightarrow \pi\pi N$ reaction describing the exchanges of Δ and N_* along with the OPE mechanism. The contribution of the latter contains 4 independent low energy parameters (up to $O(k^4)$ order). The terms of the polynomial background are added to stand for far resonances and for contact terms originating from the off-mass-shell interactions. These terms are introduced with the account of isotopic, crossing, C , P and T symmetries of strong interactions.

The data consisting of total cross sections in the energy region $0.300 \leq P_{\text{Lab}} \leq 500$ MeV/c and 1D distributions from the bubble-chamber experiments for three reaction channels were undergoing fittings to determine free parameters of the amplitude. The best solutions are characterized by $\chi_{\text{DF}}^2 = 1.16$. At the considered energies the isobar exchanges are found to be more important than OPE. The obtained solutions reveal the need in more precise data and/or in polarization measurements because of large correlations of isobar parameters with the OPE ones.

The theoretical solutions were used for modeling the Chew-Low extrapolation and the Olsson-Turner threshold approach. It is shown that the noncritical application of the former results in 100% theoretical errors, the extracted values being in fact the random numbers. The results of the Olsson-Turner method are characterized by significant systematic errors coming from unknown details of isobar physics.

1 Introduction

The pion–production reactions play the important role in the low energy physics of elementary particles and nuclei. The elementary processes $\pi N \rightarrow \pi\pi N$, $\gamma N \rightarrow \pi\pi N$ of pion production on nucleons are currently in the focus of investigations due to the progress of Chiral perturbation theory (ChPT) the foundation of which was created by the Weinberg’s work [81] and principal steps were done in the series of papers by Gasser and Leutwyler [32]. (For more references and reviews of this approach as well as more recent trends one can use the book by Donoghue, Golowich and Holstein [29] and the review papers by Meissner [56] and Pich [65]; a deep insight into the contemporary interpretation of ChPT and the role of spontaneous symmetry breaking is provided by a series of preprints by Leutwyler [52].)

The predictions of ChPT [32] (summary of the most interesting predictions as well as forthcoming experimental tests might be found in the talk [68]) explain the very sharp interest in the values of $\pi\pi$ –scattering lengths and other parameters of the $\pi\pi$ scattering. Since it is not possible experimentally to create the pionic target or the colliding pion beams there are only indirect ways for obtaining experimental data on the $\pi\pi$ scattering. The reactions $\pi N \rightarrow \pi\pi N$ and $K \rightarrow \pi\pi e\nu$ are considered as the most important sources of the (indirect) information on low energy characteristics of the $\pi\pi$ interaction. (The former reaction in what follows will be simply referred as $\pi 2\pi$ when possible.)

The review of methods of extracting the latter characteristics from $\pi 2\pi$ data being in use previously and details of their applications might be found in the paper [50] by Leksin. The methods considered for application to the modern experiments are the following [22].

1. The Chew–Low extrapolation procedure by Goebel, Chew and Low [33] is an apparently model–independent approach. It can provide the complete information on the $\pi\pi$ cross section provided the OPE dominates and the interval of the nucleon momentum transfer τ (which equals the mass of the virtual pion) allows an unique extrapolation. The last condition and the need for sufficient statistics shifts the region of application of the Chew–Low procedure to rather large values of energy ($\approx 1 - 4$ GeV). When comparing the phase space of momentum transfer $-20\mu^2 < \tau < -0.2\mu^2$ at $P_{\text{Lab}} = 500$ MeV/c with the distance of extrapolation $\approx \mu^2$ it becomes obvious that provided there are enough statistics, the kinematics of the $\pi 2\pi$ reaction itself does not prevent the use of the Chew–Low procedure at much smaller energies. It is the presence of contributions like that of Δ and N_* isobars which makes a straightforward extrapolation difficult at moderate energies due to the perturbation of the simple τ –dependence of the OPE graph. The absolute values of all other contributions are killed at the extrapolation point $\tau = \mu^2$, but the result of extrapolation is known to be sensitive to the shape of the extrapolating curve [55, 50].

2. In view of importance of concurrent mechanisms at intermediate energies the approach might be changed to determining the OPE parameters directly in the physical region of the reaction — this was implemented by the model of Oset and Vicente–Vacas [63]. It is clear that the neglect of a specific resonance contribution and/or the account of another one are capable to provide a lot of derivatives of the Oset–Vicente model.

There is the energy region below $P_{\text{Lab}} = 500$ MeV/c, where the variation of τ is sufficient to detect the OPE contribution since the contributions of the concurrent processes (being

nonnegligent) are smooth enough. The model [21] takes these features into account and naturally completes the Oset–Vicente approach in this specific energy domain.

3. The investigations by Olsson and Turner [60] are confined to the threshold of $\pi 2\pi$ reactions. Since the phase space of τ variable shrinks to the point $\tau_0 = -2.31\mu^2$ the application of the Chew–Low procedure is impossible there. The idea is to take advantage of Chiral Dynamics at the $\pi 2\pi$ threshold.

The important results of the approach are the formulae expressing the $\pi\pi$ –scattering lengths in terms of the threshold characteristics of the pion–production reactions. These formulae have gained a broad scale of application, especially in the recent years when new data on the $\pi N \rightarrow \pi\pi N$ reactions in the close–to–threshold energy region became available [42, 41, 43, 44], [72, 53, 66].

The evidence of the importance of next–to–leading order terms of Chiral Lagrangian for the πN interaction and, in particular, for the $\pi 2\pi$ amplitude [56], makes it necessary to modify the Olsson–Turner method. Recently the approach of heavy baryon approximation was used to derive corrections to the Olsson–Turner formulae and to make direct predictions of ChPT for the threshold $\pi 2\pi$ amplitude itself [11].

The recent results [47] of the so called Generalized ChPT approach [77] and the progress in the two–loop ChPT calculations [14, 47] are claiming for more precise experimental information on the $\pi\pi$ interaction at low energies at $O(k^6)$ order. Some experiments listed in ref. [68] had already been finished: BNL and LAMPF results on total cross sections have been published [53], [66], 1D-distributions have appeared recently in the WWW (home pages

<http://helena.phys.virginia.edu/~pipin/E1179/E1179.html>,

<http://helena.phys.virginia.edu/~pipin/E857/E857.html>),

higher distributions are in progress, the off–line treatment of experimental tapes of the TRI-UMF experiment [75] will be completed soon. Therefore, it is timely to make the solution which theoretical method from the above list is capable to provide more reliable treatment of the modern $\pi 2\pi$ experiments.

The main goal of the present work is to provide grounds for comparison of the listed approaches. For this purpose we develop the most extensive phenomenological amplitude of the considered reaction suitable for near–threshold and intermediate energy regions.

We are basing on the approach **2.** since both the Chew–Low extrapolation and the Olsson–Turner threshold formulae can not provide any hint for cross–checking of the rest methods. We try to fix the phenomenological amplitude by fitting the data on total cross sections and distributions of the reaction in question in the energy region from threshold up to $P_{\text{Lab}} \leq 500$ MeV/c.

To avoid any doubt in the results in respect to correctness of acceptances, systematic errors, etc. the distribution data are chosen to be the bubble–chamber ones. This leaves us with rather old experiments (which are discussed in sect. 3). However, the significant part of the data has never been published and most its part eluded strong theoretical analysis (apart authors’ checks of some isobar–like models). Therefore, it seems important to develop the tools of theoretical treatment of such data for determination of characteristics of pion–pion and pion–nucleon interactions along with other parameters of the phenomenological

amplitude.

It is worth noting that the considered reaction via unitarity relations is directly connected to the fundamental process of elastic pion–nucleon scattering at intermediate energies and other processes like $\gamma N \rightarrow \pi\pi N$ which gain the raising interest in the ChPT approach. It also enters the description of pion–nuclei scattering as an elementary process. Therefore, the structure of $\pi 2\pi$ amplitude is of great importance for nuclear and particle physics.

The paper is organized as follows. The content of sect. 2 reminds the basics of the low energy phenomenology of the $\pi N \rightarrow \pi\pi N$ reaction and describes the structure of our amplitude. Sect. 3 provides the summary of experimental data on distributions and total cross sections which we are analyzing. Sect. 4 is devoted to specifics of the fitting procedure and main results of analysis. The results of modeling the Olsson–Turner and Chew–Low approaches are exposed in sects. 5, 6 along with the discussion of some properties of our amplitude and theoretical solutions. The summary, the concluding remarks and the discussion of the perspectives of the further development are given in Conclusions.

2 Model of $\pi N \rightarrow \pi\pi N$ Amplitude

The principal features of the near-threshold phenomenology of the $\pi N \rightarrow \pi\pi N$ reaction had been already discussed in the paper [21]; in the quoted work the smooth background amplitude (+ the OPE one) had been derived for the energy domain bounded by the reaction threshold and the threshold $P_{\text{Lab}} \approx 500$ MeV/c of the Δ -isobar creation in the final state. However, the statistically significant data on $\pi 2\pi$ distributions (described in the next section) exist just for the boundary (and slightly above) of the pointed energy region. This makes necessary to modify the amplitude elaborated in ref. [21] since the smoothness assumption is hardly to be valid there.

In the current section we recall the phenomenology of $\pi 2\pi$ processes to be taken into account (subsect. 2.2) and principal parts of the modified amplitude (subsect. 2.3) the parameters of which must be determined from the data fittings. We start with the brief description of the spin-isospin structure of the discussed amplitude.

2.1 $\pi N \rightarrow \pi\pi N$ Amplitude

2.1.1 General Structure

In the isotopic space the amplitude $M_{\beta\alpha}^{abc}(\lambda_f; \lambda_i)$ of the reaction

$$\pi^a(k_1) + N_\alpha(p; \lambda_i) \rightarrow \pi^b(k_2) + \pi^c(k_3) + N_\beta(q; \lambda_f) \quad (1)$$

has 4 degrees of freedom and might be expressed either in terms of the definite isospin amplitudes or in terms of the isoscalar ones. Separating the nucleon spinor wave functions

$$M_{\beta\alpha}^{abc}(\lambda_f; \lambda_i) = \bar{u}(q; \lambda_f) \hat{M}_{\beta\alpha}^{abc}(i\gamma_5) u(p; \lambda_i) , \quad (2)$$

where the $(i\gamma_5)$ multiplier ensures the correct P -parity properties of the considered amplitude one can define the isoscalar amplitudes \hat{A} , \hat{B} , \hat{C} , \hat{D} by

$$\hat{M}_{\beta\alpha}^{abc} = \hat{A}\tau_{\beta\alpha}^a\delta^{bc} + \hat{B}\tau_{\beta\alpha}^b\delta^{ac} + \hat{C}\tau_{\beta\alpha}^c\delta^{ab} + \hat{D}i\epsilon^{abc}\delta_{\beta\alpha} . \quad (3)$$

The analysis [19] of the spinor properties of the amplitude (2) allows to express each of the isoscalar functions A, B, C, D in terms of 4 independent form factors in the crossing-covariant way

$$\begin{aligned} \hat{A} &= S_A + \bar{V}_A \hat{k} + V_A \hat{k} + i/2 T_A[\hat{k}, \hat{k}] ; \\ \hat{B} &= S_B + \bar{V}_B \hat{k} + V_B \hat{k} + i/2 T_B[\hat{k}, \hat{k}] ; \\ \hat{C} &= S_C + \bar{V}_C \hat{k} + V_C \hat{k} + i/2 T_C[\hat{k}, \hat{k}] ; \\ \hat{D} &= S_D + \bar{V}_D \hat{k} + V_D \hat{k} + i/2 T_D[\hat{k}, \hat{k}] . \end{aligned} \quad (4)$$

Here, k, \bar{k} are the crossing-covariant combinations of pion momenta

$$k = -k_1 + \epsilon k_2 + \bar{\epsilon} k_3 ; \quad \bar{k} = -k_1 + \bar{\epsilon} k_2 + \epsilon k_3 , \quad (5)$$

where $\epsilon = \exp(2\pi i/3) = -1/2 + i\sqrt{3}/2$, $\bar{\epsilon} = \epsilon^* = -1/2 - i\sqrt{3}/2$. These combinations together with the independent crossing-invariant ones

$$Q \equiv -k_1 + k_2 + k_3 = p - q ; \quad P \equiv p + q \quad (6)$$

are used to define 5 independent crossing-covariant scalar variables

$$\begin{aligned} \tau &= Q^2 ; \quad \theta = Q \cdot k ; \quad \bar{\theta} = Q \cdot \bar{k} ; \\ \nu &= P \cdot k ; \quad \bar{\nu} = P \cdot \bar{k} , \end{aligned} \quad (7)$$

which completely determine the point in the phase space of the considered reaction. The expressions of all scalar products of particles' momenta are given in the paper [21] for the case of the unbroken isotopic symmetry. The definitions (5), (6), (7) are assumed for the physical particles (k_2 is the π^- momentum in the reactions $\{- + n\}$ and $\{- 0 p\}$; in the $\{+ 0 p\}$ case k_2 is the π^+ momentum). All actual kinematical calculations in the computer programs are being processed with the isotopic symmetry breaking due to the particles' masses — this complicates the expressions given in the quoted paper. For simplicity we shall hold on the unbroken isotopic symmetry case in the illustrations and in the discussions which follow.

The τ variable coincides with the mass of the virtual pion of the OPE graph. The 4π vertex of this graph is characterized also by the Mandelstam variables. The discussion of the off-shell dependence of the 4π vertex on these variables is given in the paper [20]. To avoid ambiguity we use only the dipion invariant mass

$$s_{\pi\pi} \equiv (k_2 + k_3)^2 \quad (8)$$

in the discussion below.

The amplitudes of the observable channels of the reactions $\pi N \rightarrow \pi\pi N$ with the convention for the normalization of the particle states adopted in [21] are provided by relations (the nontrivial statistical factors are taken into account in the cases of the $\{00n\}$ and $\{++n\}$ channels):

$$\begin{aligned} \hat{M}_{\{-+n\}} &= \sqrt{2}/2 (\hat{A} + \hat{C}) ; \quad \hat{M}_{\{00n\}} = 1/2 (\hat{A}) ; \quad \hat{M}_{\{++n\}} = 1/2 (\hat{B} + \hat{C}) ; \\ \hat{M}_{\{-0p\}} &= 1/2 (\hat{C} - 2\hat{D}) ; \quad \hat{M}_{\{+0p\}} = 1/2 (\hat{C} + 2\hat{D}) . \end{aligned} \quad (9)$$

They have the same form as in eqs. (4)

$$\hat{M}_X = S_X + \bar{V}_X \hat{k} + V_X \hat{k} + i/2 T_X [\hat{k}, \hat{k}] ; \quad X = (\{-+n\}, \{-0p\}, \{00n\}, \{++n\}, \{+0p\}) , \quad (10)$$

where the spinor structures are defined according to the expansions (9), e.g. $S_{\{-+n\}} = \sqrt{2}/2(S_A + S_C)$, etc. In practice, the following combinations of the vector structures

$$V_X^R \equiv (V_X + \bar{V}_X)/2 ; \quad V_X^I \equiv (V_X - \bar{V}_X)/(2i) \quad (11)$$

are being used in the course of calculations.

2.1.2 Cross Section

The experimental data of the channel X are compared with the theoretical cross sections $\sigma_{(\alpha)}^{\text{Th}}$ for a given experimental point (α)

$$\sigma_{(\alpha)}^{\text{Th}} = \frac{\sigma_c}{4J} \int \frac{d^3k_2}{(2\pi)^3 2k_{20}} \frac{d^3k_3}{(2\pi)^3 2k_{30}} \frac{d^3q}{(2\pi)^3 2q_0} (2\pi)^4 \delta^4(p + k_1 - q - k_2 - k_3) ||M||^2 \Theta_\alpha. \quad (12)$$

Here, $\sigma_c \equiv (\hbar c)^2 = 0.38937966(23)[\text{GeV}^2 \text{ mbarn}]$ is the conversion constant,

$$4J = 4\sqrt{(p \cdot k_1)^2 - m_p^2 \mu_1^2}$$

stands for normalization of the initial state and the characteristic function $\Theta_{(\alpha)} = \Theta_{(\alpha)}(p, k_1, q, k_2, k_3)$ of the bin (α) describes the appropriate cuts in the phase space (if any; in the case of the total cross section this function is equal to 1). The notation $||M||^2$ stands for the squared modulus of the amplitude summed over polarizations of the final nucleon and averaged over ones of the initial proton (we shall call it simply *matrix element*). The statistical factor (equal to the product of $1/n_\nu!$ over subsets of identical particles) for calculation of the cross section was included into definitions (9) of the physical reaction amplitudes.

The matrix element $||M||^2 \equiv ||M_X||^2$ is the quadratic form of the vector of spinor structures $(S_X, V_X, \bar{V}_X, T_X)$ (or, the same, of the vector (S_X, V_X^R, V_X^I, T_X)):

$$\begin{aligned} ||M_X||^2 &\equiv 1/2 \sum_{\lambda_f, \lambda_i} [\bar{u}(q; \lambda_f) \hat{M}_X(i\gamma_5) u(p; \lambda_i)] [\bar{u}(q; \lambda_f) \hat{M}_X(i\gamma_5) u(p; \lambda_i)]^* \\ &= \begin{pmatrix} S_X \\ V_X \\ \bar{V}_X \\ T_X \end{pmatrix}^\dagger G \begin{pmatrix} S_X \\ V_X \\ \bar{V}_X \\ T_X \end{pmatrix}, \quad (X = \{-+n\}, \{-0p\}, \{00n\}, \{++n\}, \{+0p\}); \end{aligned} \quad (13)$$

$$G \equiv \frac{1}{2} \text{Sp} \left[(\hat{q} + m) \begin{pmatrix} \hat{1} \\ \hat{k} \\ \hat{k} \\ \frac{i}{2}[\hat{k}, \hat{k}] \end{pmatrix} (\hat{p} - m) \gamma_0 \begin{pmatrix} \hat{1} \\ \hat{k} \\ \hat{k} \\ \frac{i}{2}[\hat{k}, \hat{k}] \end{pmatrix}^\dagger \gamma_0 \right]. \quad (14)$$

For the simplified case of equal pion masses the matrix G of the above form is given in the paper [21]. In practice, the matrix for every channel had been calculated separately with the physical masses of all particles in the considered channel.

To plot the data and the theoretical results we define the *quasi-amplitude* $\langle M_{(\alpha)} \rangle$ which is the square root of the cross section (12) divided by the phase space in the case of the total cross section data; in the case of distributions both the cross section and the phase space are independently normalized to 1 — we call this quantity *normalized quasi-amplitude* $\langle M_{(\alpha)} \rangle_{\text{norm}}$:

$$\langle M_{(\alpha)} \rangle \equiv \sqrt{\frac{\sigma_{(\alpha)}(||M||^2)}{\sigma_{(\alpha)}(1)}}, \quad \langle M_{(\alpha)} \rangle_{\text{norm}} \equiv \sqrt{\frac{\sigma_{(\alpha)}^n(||M||^2)}{\sigma_{(\alpha)}^n(1)}}. \quad (15)$$

Here, the phase space $\sigma(1)$ is the theoretical cross section (12) obtained with the unit matrix element.

2.1.3 Threshold Properties

At the threshold of the reaction there are considerable simplifications in the representations (4) or (10) since: a) the momenta of the outgoing pions are equal to each other ($\hat{k}_2 = \hat{k}_3$), b) the contribution of the \hat{D} amplitude to the amplitudes (9) becomes zero and c) $\hat{B} = \hat{C}$.

Another simplification takes place in the sum over final polarizations and the average over initial ones of the amplitude (2) squared modulus. At the threshold it degenerates to

$$\begin{aligned} \|M_X\|^2 &= (-\tau_0)[S_X^0 - (2m + 3\mu)(\bar{V}_X^0 + V_X^0)]^2, \\ (X &= \{-+n\}, \{-0p\}, \{00n\}, \{++n\}, \{+0p\}), \end{aligned} \quad (16)$$

where $\tau_0 = -3\mu^2 m / (m + 2\mu)$ is the threshold value of the variable τ . This provides the grounds to introduce the *threshold amplitudes*.

The isotopic threshold amplitudes are

$$\begin{aligned} A^0 &= \sqrt{-\tau_0}[S_A^0 - (2m + 3\mu)(\bar{V}_A^0 + V_A^0)]; \\ B^0 &= \sqrt{-\tau_0}[S_B^0 - (2m + 3\mu)(\bar{V}_B^0 + V_B^0)]; \\ C^0 &= \sqrt{-\tau_0}[S_C^0 - (2m + 3\mu)(\bar{V}_C^0 + V_C^0)], \end{aligned} \quad (17)$$

where all form factors are to be calculated at the threshold values of kinematical variables — this provides

$$B^0 = C^0. \quad (18)$$

To link the isotopic threshold amplitudes (17) with the experimental information let us construct the quantities M^0

$$\begin{aligned} M_{\{-+n\}}^0 &= (A^0 + B^0)\sqrt{2}/2, \quad M_{\{-0p\}}^0 = B^0/2, \quad M_{\{00n\}}^0 = A^0/2, \\ M_{\{++n\}}^0 &= (B^0 + C^0)/2 = B^0, \quad M_{\{+0p\}}^0 = B^0/2, \end{aligned} \quad (19)$$

which include both the isotopic and the statistical factors.

Then the absolute values of the threshold amplitudes M_X^0 might be expressed in terms of threshold limits of the experimental quasi-amplitudes (15):

$$\begin{aligned} \langle M_{\{-+n\}} \rangle_{|s \rightarrow s_0} &= |A^0 + B^0|/\sqrt{2}, \quad \langle M_{\{-0p\}} \rangle_{|s \rightarrow s_0} = |B^0|/2, \quad \langle M_{\{00n\}} \rangle_{|s \rightarrow s_0} = |A^0|/2, \\ \langle M_{\{++n\}} \rangle_{|s \rightarrow s_0} &= |B^0|, \quad \langle M_{\{+0p\}} \rangle_{|s \rightarrow s_0} = |B^0|/2. \end{aligned} \quad (20)$$

The threshold amplitudes (19) are dimensional and in the following their numerical values will be given in $[(\text{GeV})^{-1}]$.

The threshold limits (19), being determined by only two isotopic threshold amplitudes A^0 and B^0 , must satisfy three relations. The first two are straightforward:

$$|M_{\{++n\}}^0| = 2|M_{\{-0p\}}^0| = 2|M_{\{+0p\}}^0|. \quad (21)$$

From the definition (19) it follows that

$$M_{\{++n\}}^0 = \sqrt{2}M_{\{-+n\}}^0 - 2M_{\{00n\}}^0 . \quad (22)$$

This implies that, depending on the relative sign of A^0 and B^0 , the relation between positive quantities (20) might be either

$$|M_{\{++n\}}^0| = \sqrt{2}|M_{\{-+n\}}^0| - 2|M_{\{00n\}}^0| \quad (23)$$

or

$$|M_{\{++n\}}^0| = \sqrt{2}|M_{\{-+n\}}^0| + 2|M_{\{00n\}}^0| \quad (24)$$

or

$$|M_{\{++n\}}^0| = -\sqrt{2}|M_{\{-+n\}}^0| + 2|M_{\{00n\}}^0| . \quad (25)$$

Now it is necessary to recall the known properties of $\pi 2\pi$ cross sections. Since in the near threshold region the known cross sections $\sigma_{\{00n\}}$ of the $\{0\ 0\ n\}$ channel are approximately equal to the cross sections $\sigma_{\{-+n\}}$ this excludes the possibility (23) because it results in the negative RHS. In the whole region $P_{\text{Lab}} \leq 0.5\text{GeV}/c$ the cross sections $\sigma_{\{++n\}}$ are considerably smaller than $\sigma_{\{-+n\}}$ and/or $\sigma_{\{00n\}}$; so, the variant (24) is impossible. Thus, combining with the previous two relations, we can state:

$$2|M_{\{-0p\}}^0| = 2|M_{\{+0p\}}^0| = |M_{\{++n\}}^0| = 2|M_{\{00n\}}^0| - \sqrt{2}|M_{\{-+n\}}^0| . \quad (26)$$

2.1.4 Remarks on Sign Ambiguity

To resume the discussion of the general structure of the $\pi 2\pi$ amplitude let us consider briefly the problem of the sign ambiguity in the theoretical amplitude which is used to fit the experimental cross section data. The examination of relations (20) shows that already in this simplified threshold case apart the overall sign ambiguity of isotopic threshold amplitudes A^0 , B^0 their relative sign might also become indefinite depending on the accuracy of the experimental information.

In what follows we call the solution *physical* (*unphysical*) when A^0 and B^0 are of different (equal) signs. In terms of the $\pi\pi$ -scattering lengths the two cases of signs correspond to the different (equal) signs of $a_0^{I=0}$ and $a_0^{I=2}$.

In general there are no grounds to wait for a simplification to take place at a distance from the threshold. Indeed, the expression (13) for the matrix element $\|M_X\|^2$ might be brought to the diagonal form (for example, in terms of the analogues of the diagonal derivative amplitudes of Rebbi [69]) in which it becomes the sum of four squared modules of the orthogonal amplitudes. The abundance of solutions found in the course of data fittings should be explained in part by a variety of choices of the signs in the above four terms in the cross section of every channel.

2.2 Near-Threshold $\pi N \rightarrow \pi\pi N$ Phenomenology Guidelines

1. The current knowledge of physics of the pion-nucleon interactions provides no evidence of possible mechanisms or processes resulting in the strong variation of the amplitude of the $\pi N \rightarrow \pi\pi N$ reaction in the phase space at energies up to $\approx 2m_\pi$ above threshold. All resonances but N_* and Δ are located outside the phase space.

2. The contribution of the near-threshold Δ pole is only due to the chain $\pi N \rightarrow \Delta \rightarrow \pi\pi N$. It is suppressed 1) by the negligible width of the decay $\Delta \rightarrow \pi\pi N$; 2) by Quantum mechanics: Δ is located precisely at the $\pi 2\pi$ threshold where the process $\pi N \rightarrow \pi\pi N$ must proceed through the waves P_{11} and P_{31} of the initial pion-nucleon system (in the L_{2I2J} notation) while Δ can be created only in the P_{33} wave of the π - N system.

3. The closest to the phase space contribution of the meson-resonance type is that of OPE — all the other are very distant at the discussed energies.

4. The tails of resonances result in some constant background in the physical domain and, at most, in some slow variation of the amplitude. (One would need the extraordinary precision of experimental data to distinguish between a linear function in the corresponding variable and the far pole.)

5. The number of free (or unknown) parameters in $\pi\pi$, πN , $\pi\Delta$, πN_* interactions exceeds the number of degrees of freedom of the smooth near-threshold amplitude.

6. All resonances contribute with terms built of various scalar products of momenta. There are at most five such products which might be considered to be independent or, the same, they are built of five invariant variables (at the fixed initial energy, four variables left). Hence, the arbitrary linear function is parametrized with 6 parameters: a constant + 5 coefficients at linear variables. This applies to any of 4 independent isospin amplitudes which describe 5 observable channels of the reaction.

7. There are four different spinor structures in the $\pi 2\pi$ amplitude. Even in the case of the unpolarized experiment they provide the specific dependence on variables which might well be nonnegligent at some distance from the threshold.

8. The Bose statistics, the isospin symmetry, the C -invariance and the crossing, being the exact properties of the amplitude derived according to the rules of the quantum field theory, restrict the amplitude dependence on variables, making some parameters vanish and relating the rest parameters.

9. As a result there might be about 20 parameters for the near-threshold description of all channels and, in particular, no more than 15 for the case of the $\pi^- p \rightarrow \pi^- \pi^+ n$ process. By the unitarity conditions which relate the nonvanishing $\pi 2\pi$ isospin amplitudes only with the P_{31} and P_{11} waves of elastic πN amplitudes, the above parameters must be approximately real. Only few of 20 imaginary parts of the polynomial background are expected to be of importance.

10. The discussed structures must be combined with the explicit term describing the OPE amplitude and isobar contributions. This will provide about 20 additional parameters if D waves of the $\pi\pi$ scattering and all structures of the vertices $\pi\pi N\Delta$, $\pi\pi N_*\Delta$, $\pi\pi NN_*$ are important.

$SE_{\pi N}$	$I(J^P)$	$SE_{\pi\pi}$	$I^G(J^{PC_n})$	SE_{NN}	$I^G(J^{PC_n})$
$N = (p, n)$	$\frac{1}{2}(\frac{1}{2}^+)$	$\sigma = f_0(400-1200)$	$0^+(0^{++})$	$\pi = (\pi^\pm, \pi^0)$	$1^-(0^{-+})$
$\Delta = \Delta(1232)$	$\frac{3}{2}(\frac{3}{2}^+)$	$\rho = \rho(770)$	$1^+(1^{--})$	$\omega = \omega(782)$	$0^-(1^{--})$
$N_* = N(1440)$	$\frac{1}{2}(\frac{1}{2}^+)$	$f = f_2(1270)$	$0^+(2^{++})$	$A = a_1(1260)$	$1^-(1^{++})$
$N' = N(1520)$	$\frac{1}{2}(\frac{3}{2}^-)$	$\rho' = \rho(1450)$	$1^+(1^{--})$	$\pi' = \pi(1300)$	$1^-(0^{-+})$
$\mathcal{N} = N(1535)$	$\frac{1}{2}(\frac{1}{2}^-)$	\dots		\dots	
\dots					

Table 1: Resonances and particles from PDG-96 [70] responsible for pole contributions to the low energy $\pi N \rightarrow \pi\pi N$ amplitude.

11. The cuts due to thresholds of another inelastic processes like the 3π production, the η production, etc. are conspired by nearby isobars.

12. The analysis of the paper [54] makes it evident that isobar resonances saturate the existing data on total cross sections below 1 GeV. Therefore, the imaginary part of the $\pi 2\pi$ amplitude might be described by the Breit–Wigner form of isobar contributions and the discussed above parameters of the imaginary background might appear to be negligible.

2.3 Resonance Contributions to $\pi N \rightarrow \pi\pi N$ Amplitude

The $\pi 2\pi$ amplitude to be developed must cover the energy interval from the threshold to the isobar region. Therefore, the approach **2** mentioned in Introduction is the most suitable one for the discussed purpose since it admits the due account of isobar physics and can provide the maximal model independence of the obtained results.

Let us first enumerate the resonance–exchange graphs which are proper to our reaction (it is suitable to use the two–particle channel for labelling). Three representatives $SE_{\pi N}$, $SE_{\pi\pi}$, SE_{NN} of inequivalent crossing–related single–pole graphs are shown in Fig. 1. Every four–particle vertex of the above graphs can be expanded in at most two different ways providing no more than three types of inequivalent double–pole graphs which we mark in $DE_{\pi N, \pi N}$, $DE_{\pi N, \pi\pi}$, $DE_{NN, \pi\pi}$ (see Fig. 1). In what follows we shall use the self–explanatory notations like $SE_{\pi N}\{\Delta\}$, $DE_{NN, \pi\pi}\{\omega, \rho\}$ when discussing contributions of classes of crossing–related graphs. It is evident that all distinct resonances and particles responsible for pole contributions to the amplitude enter already the single–pole scheme; the particles which might be relevant to the intermediate energy amplitude are listed in the Table 1. There are enough representatives of the lowest spin–isospin states in the lists $SE_{\pi\pi}$, SE_{NN} . In the case of the $SE_{\pi N}$ channel the list is far from being complete. In the present paper we limit ourselves by contributions from particles N , Δ , N_* , σ , ρ , π , ω and A ; in fact, the interactions of σ , ω and A given below in the lists of lagrangians for the purpose of the forthcoming discussion were omitted from the actual analysis.

Apart the OPE contribution our model is described by the effective interaction lagrangian which is used to construct the tree–level amplitude; all terms of the lagrangian are collected

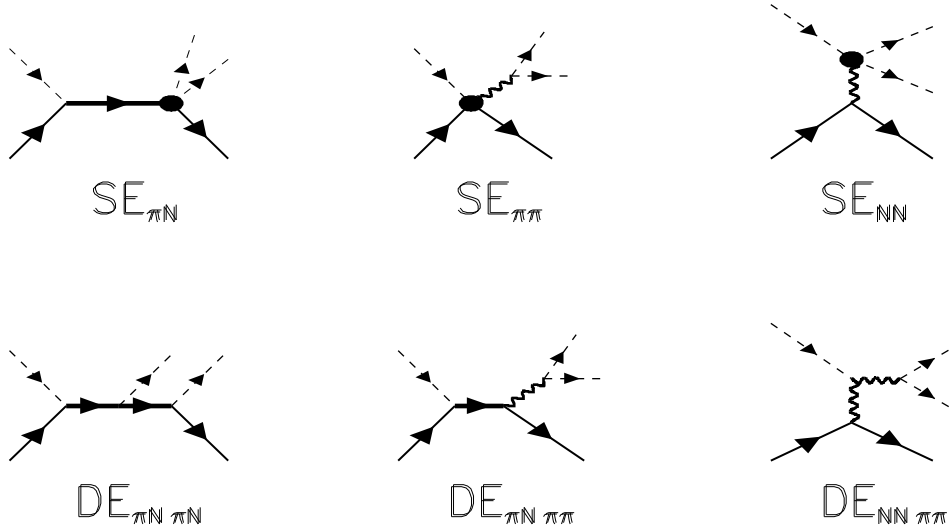


Figure 1: Representatives of graphs of resonance contributions.

in Tables 2, 3. In general, we are trying to use the minimal derivative coupling especially when particles of the nontrivial spin (for example, in the $\rho N\Delta$ vertex) are being involved. In the contrary case the terms of too high order in the momentum are inevitable to be present in the amplitude. However, in the case of the three-particle vertices containing the pion, like πNN , $\pi N\Delta$, etc., the vertices are brought to the derivative-coupling form. Having in mind the complete equivalence of nonderivative and derivative couplings in such vertices (in the difference of the corresponding amplitudes the propagators always become contracted) we assume that only other types of vertices (for example, 4π , $\pi\pi NN$, etc.) are responsible for the explicit breaking of Chiral Symmetry.

Even in the brief summary of properties of the considered interactions we must point that the form of the four-particle vertices is chosen to represent all spin-isospin structures of the given vertex. This makes impossible to fix the lagrangian parameters from the decay data (for example, the known width for $N_* \rightarrow \pi\pi N$ provides only bounds for 4 parameters of the $\pi\pi NN_*$ lagrangian given in the Table 2). However, we prefer to avoid any doubt in respect to a possible model dependence of the results for $\pi\pi$ -scattering lengths or, at least, to leave a chance to check the presence of such dependence.

The central contribution to our amplitude is supposed to come from the OPE graph $SE_{NN}(\pi)$. It is parametrized basing on the cross-symmetric threshold expansion of the 4π vertex elaborated in the paper [23]. Apart the account of the imaginary part the expansion in the $O(k^4)$ order is equivalent to the form described in the papers [19, 21]. The results of

Graph [Vertex]	Lagrangian
$\text{SE}_{\pi N}\{N\}$ [$\pi\pi NN$]	$g_{\pi\pi NN}^1 \bar{N} \delta_{ab} N \pi^a \pi^b + g_{\pi\pi NN}^2 \bar{N} \delta_{ab} N \partial^\mu \pi^a \partial_\mu \pi^b$ $+ g_{\pi\pi NN}^3 \bar{N} i \epsilon_{abc} \tau^c \gamma_\mu N [\partial^\mu \pi^a \pi^b - \pi^a \partial^\mu \pi^b]$ $+ g_{\pi\pi NN}^4 \bar{N} i \epsilon_{abc} \tau^c [\gamma_\mu, \gamma_\nu] N \partial^\mu \pi^a \partial^\nu \pi^b$
$\text{SE}_{\pi N}\{N_*\}$ [$\pi\pi NN_*$]	$g_{\pi\pi NN_*}^1 \bar{N} \delta_{ab} N_* \pi^a \pi^b + g_{\pi\pi NN_*}^2 \bar{N} \delta_{ab} N_* \partial^\mu \pi^a \partial_\mu \pi^b$ $+ g_{\pi\pi NN_*}^3 \bar{N} i \epsilon_{abc} \tau^c \gamma_\mu N_* [\partial^\mu \pi^a \pi^b - \pi^a \partial^\mu \pi^b]$ $+ g_{\pi\pi NN_*}^4 \bar{N} i \epsilon_{abc} \tau^c [\gamma_\mu, \gamma_\nu] N_* \partial^\mu \pi^a \partial^\nu \pi^b + \{\text{H.C.}\}$
$\text{SE}_{\pi N}\{\Delta\}$ [$\pi\pi N\Delta$]	$\bar{N} (g_{\pi\pi N\Delta}^1 F_{dbc}^0 + 3g_{\pi\pi N\Delta}^2 F_{dbc}^1) i \gamma_5 \Delta_\mu^d \partial^\mu \pi^b \pi^c$ $+ \bar{N} (g_{\pi\pi N\Delta}^3 F_{dbc}^0 + 3g_{\pi\pi N\Delta}^4 F_{dbc}^1) \gamma_\nu \gamma_5 \Delta_\mu^d \partial^\mu \pi^b \partial^\nu \pi^c + \{\text{H.C.}\};$ $F_{dbc}^0 = i \epsilon_{dbc} + \delta_{db} \tau_c - \delta_{dc} \tau_b; \quad F_{dbc}^1 = \delta_{db} \tau_c + \delta_{dc} \tau_b - 2/3 \delta_{bc} \tau_d$
$\text{SE}_{NN}\{\pi\}$ [$\pi\pi\pi\pi$]	$V_{4\pi}$
$\text{SE}_{NN}\{\omega\}$ [$\pi\pi\pi\omega$]	$g_{\pi\pi\pi\omega} \omega_\mu \partial_\nu \pi^a \partial_\alpha \pi^b \partial_\beta \pi^c i \epsilon_{abc} i \epsilon^{\mu\nu\alpha\beta}$
$\text{SE}_{NN}\{A\}$ [$\pi\pi\pi A$]	$g_{\pi\pi\pi A}^1 A_b^\mu \pi^b \pi^a \partial_\mu \pi^a$ $+ g_{\pi\pi\pi A}^2 A_b^\mu \partial_\mu \pi^b \partial_\nu \pi^a \partial^\nu \pi^a + g_{\pi\pi\pi A}^3 A_b^\mu \partial_\nu \pi^b \partial_\mu \pi^a \partial^\nu \pi^a$
$\text{SE}_{\pi\pi}\{\sigma\}$ [$\pi\sigma NN$]	$g_{\pi\sigma NN} \bar{N} \tau^a \gamma_\mu \gamma_5 N \partial^\mu \pi_a \sigma$
$\text{SE}_{\pi\pi}\{\rho\}$ [$\pi\rho NN$]	$g_{\pi\rho NN}^1 \bar{N} \gamma_\mu \gamma_\nu \gamma_5 N (\partial^\mu \pi_a \rho_a^\nu - \partial^\nu \pi_a \rho_a^\mu) / 2$ $+ g_{\pi\rho NN}^2 \bar{N} \tau^a \gamma_5 N \partial_\mu \pi_b \rho_c^\mu i \epsilon_{abc}$

Table 2: Lagrangians for 4-particle vertices of the SE graphs.

the present work which will be discussed below confirm that the precision of the currently available experimental data does not allow to consider higher terms of the $\pi\pi$ amplitude.

We list in Tables 2, 3 below the interactions most part of which had been used for the construction of the phenomenological amplitude entering the data fittings. Since all 3-particle vertices of the SE series of graphs are present also in the DE graphs we do not describe them separately — see Table 3. In Table 2 the symbol $V_{4\pi}$ stands for the $\pi\pi$ interaction — this contribution is taken in the direct amplitude form.

Graph [Vertex]	Lagrangian
$\text{DE}_{\pi N, \pi N} \{N, N\}$ [πNN]	$g_{\pi NN} \bar{N} \tau_a \gamma_\mu \gamma_5 N \partial^\mu \pi^a$
$\text{DE}_{\pi N, \pi N} \{N, N_*\}$ [πNN_*]	$g_{\pi NN_*} \bar{N} \tau_a \gamma_\mu \gamma_5 N_* \partial^\mu \pi^a + \{\text{H.C.}\}$
$\text{DE}_{\pi N, \pi N} \{N, \Delta\}$ [$\pi N\Delta$]	$g_{\pi N\Delta} (\bar{\Delta}_\mu^a P_{ab} N \partial^\mu \pi^b + \bar{N} P_{ab}^\dagger \Delta_\mu^a \partial^\mu \pi^b)$
$\text{DE}_{\pi N, \pi N} \{N_*, N_*\}$ [$\pi N_* N_*$]	$g_{\pi N_* N_*} \bar{N}_* \tau_a \gamma_\mu \gamma_5 N_* \partial^\mu \pi^a$
$\text{DE}_{\pi N, \pi N} \{N_*, \Delta\}$ [$\pi N_* \Delta$]	$g_{\pi N_* \Delta} (\bar{\Delta}_\mu^a P_{ab} N_* \partial^\mu \pi^b + \bar{N}_* P_{ab}^\dagger \Delta_\mu^a \partial^\mu \pi^b)$
$\text{DE}_{\pi N, \pi N} \{\Delta, \Delta\}$ [$\pi \Delta \Delta$]	$g_{\pi \Delta \Delta} \bar{\Delta}_\mu^a \gamma_\nu \gamma_5 A_{abc} \bar{\Delta}_\mu^b \partial^\nu \pi^c,$ $A_{abc} = \frac{4}{9} (-2\delta_{bc} \tau_a - 2\delta_{ac} \tau_b + 8\delta_{ab} \tau_c - 5i\epsilon_{abc})$
$\text{DE}_{\pi N, \pi \pi} \{N, \sigma\}$ [σNN]	$g_{\sigma NN} \bar{N} N \sigma$
$\text{DE}_{\pi N, \pi \pi} \{N, \rho\}$ [ρNN]	$g_{\rho NN}^V \bar{N} \gamma_\mu \tau^a N \rho_a^\mu + g_{\rho NN}^T \bar{N} \sigma_{\mu\nu} \tau^a N \partial^\mu \rho^\nu$
$\text{DE}_{\pi N, \pi \pi} \{N_*, \sigma\}$ [σNN_*]	$g_{\sigma NN_*} \bar{N} N_* \sigma + \{\text{H.C.}\}$
$\text{DE}_{\pi N, \pi \pi} \{N_*, \rho\}$ [ρNN_*]	$g_{\rho NN_*}^V \bar{N} \gamma_\mu \tau^a N_* \rho_a^\mu + g_{\rho NN_*}^T \bar{N} \sigma_{\mu\nu} \tau^a N_* \partial^\mu \rho^\nu + \{\text{H.C.}\}$
$\text{DE}_{\pi N, \pi \pi} \{\Delta, \rho\}$ [$\rho N\Delta$]	$g_{\rho N\Delta} \bar{\Delta}_\mu^a P_{ab} N \rho^{\mu b} + \{\text{H.C.}\}$
$\text{DE}_{NN, \pi \pi} \{\pi, \sigma\}$ [$\pi \pi \sigma$]	$g_{\pi \pi \sigma} \sigma \partial_\mu \pi^a \partial^\mu \pi^a$
$\text{DE}_{NN, \pi \pi} \{\pi, \rho\}$ [$\pi \pi \rho$]	$g_{\pi \pi \rho} \partial^\nu \rho_a^\mu \partial_\nu \pi^b \partial_\mu \pi^c \epsilon_{abc}$
$\text{DE}_{NN, \pi \pi} \{\omega, \rho\}$ [$\pi \rho \omega$] [ωNN]	$g_{\pi \rho \omega} \omega_\mu \partial_\nu \pi^a \partial_\alpha \rho_\beta^a i \epsilon^{\mu\nu\alpha\beta}$ $g_{\omega NN}^V \bar{N} \gamma_\mu N \omega^\mu + g_{\omega NN}^T \bar{N} \sigma_{\mu\nu} N \partial^\mu \omega^\nu$
$\text{DE}_{NN, \pi \pi} \{A, \sigma\}$ [$\pi \sigma A$]	$g_{\pi \sigma A} A_a^\mu \partial_\mu \pi^a \sigma$
$\text{DE}_{NN, \pi \pi} \{A, \rho\}$ [$\pi \rho A$] [ANN]	$[g_{\pi \rho A}^1 \partial^\mu \pi^a \partial_{[\mu} \rho_{\nu]}^b A^{\nu c} + g_{\pi \rho A}^2 \partial^\mu \pi^a \rho^{\nu b} \partial_{[\mu} A_{\nu]}^c] i \epsilon_{abc}$ $g_{ANN}^V \bar{N} \gamma_\mu \gamma_5 \tau^a N A_a^\mu + g_{ANN}^T \bar{N} \sigma_{\mu\nu} \gamma_5 \tau^a N \partial^\mu A^\nu$

Table 3: Lagrangians for 3-particle vertices of the DE graphs.

2.4 Background Contribution to $\pi N \rightarrow \pi\pi N$ Amplitude

An important issue of the approach [19, 21] developed for the near-threshold energy region is given by the linear background terms presented in the form that respects the symmetries of strong interactions, namely, P , C , T , $SU_F(2)$ and crossing. To modify this ingredient of the model we need first to discuss the role of these smooth terms in the amplitude.

Initially, such terms were added to the OPE ones to stand for all other possible mechanisms of the $\pi N \rightarrow \pi\pi N$ reaction. When taking into account only a part of contributions of particles listed in Table 1 one leaves enough room for the background terms standing for the rest resonances.

Another reason for the presence of a background is connected with ambiguities which are specific to the off-shell interactions of high-spin particles (see, for example, the old discussion [36, 59, 62]). These interactions result in polynomial terms in the considered amplitude (and polynomial terms in the 4-particle vertices). The overall contribution of this kind coming from all resonances is constrained by the asymptotic conditions for the entire amplitude. In principle, this makes necessary to use the consistent theory for particle propagators and all vertices (like πNN , $\pi N\Delta$, etc.). Leaving the parameters of the polynomial background free we are safe to use the propagators and the vertices in the form determined by the simplicity reasons and/or by the chiral-symmetry arguments. (In particular, we are using the simplest form

$$S_M^{\mu'\mu}(k) = \frac{1}{3M^2} \left[-3M^2 g^{\mu'\mu} + M^2 \gamma^{\mu'} \gamma^\mu + 2k^{\mu'} k^\mu - M(k^{\mu'} \gamma^\mu - \gamma^{\mu'} k^\mu) \right] \quad (27)$$

for the nominator of the propagator of a $(3^+/2)$ particle.)

Since we are regularizing the exchange graphs which have poles in the physical region by the $iM\Gamma$ shift in the propagators the polynomial background must have both real and imaginary parts.

The discussed nature of the background terms forces us to modify the model of the papers [19, 21] in two directions. First, we add the second order terms in variables (7) into the scalar structures S_A , S_B , S_C , S_D :

$$\begin{aligned} S_A^{(2)} &\equiv S_A^{(2)}(\tau, \nu, \bar{\nu}, \theta, \bar{\theta}) \\ &= A_{12}\tau^2 + A_{13}\bar{\nu}\nu + A_{14}\bar{\theta}\theta + A_{15}(\nu^2 + \bar{\nu}^2) + A_{16}(\theta^2 + \bar{\theta}^2) + A_{17}\tau(\theta + \bar{\theta}); \end{aligned} \quad (28)$$

$$S_B^{(2)} = S_A^{(2)}(\tau, \bar{\epsilon}\nu, \epsilon\bar{\nu}, \bar{\epsilon}\theta, \epsilon\bar{\theta}); \quad S_C^{(2)} = S_A^{(2)}(\tau, \epsilon\nu, \bar{\epsilon}\bar{\nu}, \epsilon\theta, \bar{\epsilon}\bar{\theta}); \quad (29)$$

$$S_D^{(2)} = A_{18}i(\nu\bar{\theta} - \theta\bar{\nu}). \quad (30)$$

(This makes the dimensions of the tensor and the scalar structures of the decomposition (4) balanced.)

Second, all 18 terms of the *real* background (11 of which are described in the paper [21] and the rest are given by eqs. (28)–(30)) had been copied to provide the *imaginary* background of the amplitude.

Let us now clarify the concept of *contribution* which we are widely using throughout the paper. From the point of view of Chiral Dynamics the usage of notions like the background

contribution (a part of which the so called contact terms are), the contribution of OPE, etc. is meaningless since the field redefinition does not allow a separate graph to be well-defined — see the relevant discussion in the book [29]. The absence of the common solution on the role of the higher-spin baryons in ChPT makes the above notions even more ambiguous. Nevertheless, such quantities as the residues of the poles and the on-shell parameters of $V_{4\pi}$ are well-defined — these very quantities are in the focus of our project. As for the off-mass-shell contributions, in particular, the OPE one, we take them as they are, the Lagrangian source and Feynman rules providing the model-dependent answer. The field redefinition then modifies, first, the polynomial background terms and, second, the parameters of SE graphs. It has been already pointed out that we are leaving the background parameters free (and keeping all spin-isospin structures of 4-particle vertices being represented) — this helps to avoid the dependence of the results on a particular model.

To summarize, the considered amplitude contains 36 free parameters of the polynomial background, 4 free parameters of the real part of the OPE contribution and 5 formal parameters of its imaginary part (their relations with parameters of the real part are described in the paper [23]) and parameters from the lists of Table 2 and Table 3 discussed in the previous subsection. In the current paper we shall discuss the fittings performed with 21 parameters from the above lists coming from the exchanges $SE_{\pi N}(N)$, $SE_{\pi N}(\Delta)$, $SE_{\pi N}(N_*)$, $SE_{\pi\pi}(\rho)$, $DE_{\pi N, \pi N}\{N, N\}$, $DE_{\pi N, \pi N}\{N, \Delta\}$, $DE_{\pi N, \pi N}\{N, N_*\}$, $DE_{\pi N, \pi N}\{N_*, N_*\}$, $DE_{\pi N, \pi N}\{N_*, \Delta\}$, $DE_{\pi N, \pi N}\{\Delta, \Delta\}$ only. For the purpose of the forthcoming discussion we need to enumerate the fitting parameters — this is done in Table 4 below. The background parameters A_1 – A_{18} and their analogs i_{19} – i_{36} in the imaginary part of the amplitude have been already discussed in the previous subsection; these parameters had been being processed in fittings as they are — to save space we do not list them once more. Some factors were absorbed into the fitting parameters to improve running characteristics of the code. The list of expressions of the actual fitting parameters in terms of the constants of the interaction Lagrangian is presented in Table 4.

Graph	Fitting Parameter	Expression
$SE_{NN}\{\pi\}$	o_1	$2g_{\pi NN} \cdot g_0$
	o_2	$2g_{\pi NN} \cdot g_1$
	o_3	$2g_{\pi NN} \cdot g_2$
	o_4	$2g_{\pi NN} \cdot g_3$
$SE_{\pi\pi}\{\rho\}$	r_1	$g_{\pi\rho NN}^1 \cdot g_{\pi\pi\rho}$
	r_2	$g_{\pi\rho NN}^2 \cdot g_{\pi\pi\rho}$
$DE_{\pi N, \pi\pi}\{N, \rho\}$	r_3	$g_{\rho NN}^V \cdot g_{\pi NN} \cdot g_{\pi\pi\rho}$
$SE_{\pi N}\{\Delta\}$	D_1	$g_{\pi N\Delta} \cdot g_{\pi\pi N\Delta}^1$
	D_2	$g_{\pi N\Delta} \cdot g_{\pi\pi N\Delta}^2$
	D_3	$g_{\pi N\Delta} \cdot g_{\pi\pi N\Delta}^3$
	D_4	$g_{\pi N\Delta} \cdot g_{\pi\pi N\Delta}^4$
$DE_{\pi N, \pi N}\{\Delta, \Delta\}$	D_5	$16(g_{\pi N\Delta})^2 \cdot g_{\pi\Delta\Delta}/9$
$DE_{\pi N, \pi N}\{N, \Delta\}$	D_6	$(g_{\pi N\Delta})^2 \cdot g_{\pi NN}/3$
$SE_{\pi N}\{N_*\}$	R_1	$g_{\pi NN_*} \cdot g_{\pi\pi NN_*}^1$
	R_2	$g_{\pi NN_*} \cdot g_{\pi\pi NN_*}^2$
	R_3	$2g_{\pi NN_*} \cdot g_{\pi\pi NN_*}^3$
	R_4	$g_{\pi NN_*} \cdot g_{\pi\pi NN_*}^4$
$DE_{\pi N, \pi N}\{N_*, N_*\}$	R_5	$g_{\pi N_* N_*} \cdot (g_{\pi NN_*})^2/8$
$DE_{\pi N, \pi N}\{N_*, \Delta\}$	R_6	$g_{\pi N\Delta} \cdot g_{\pi N_*\Delta} \cdot g_{\pi NN_*}/3$
$DE_{\pi N, \pi N}\{N, N_*\}$	R_7	$g_{\pi NN} \cdot (g_{\pi NN_*})^2/8$
$SE_{\pi N}\{N\}$	N_1	$g_{\pi NN} \cdot g_{\pi\pi NN}^1$
	N_2	$g_{\pi NN} \cdot g_{\pi\pi NN}^2$
	N_3	$2g_{\pi NN} \cdot g_{\pi\pi NN}^3$
	N_4	$g_{\pi NN} \cdot g_{\pi\pi NN}^4$
$DE_{\pi N, \pi N}\{N, N\}$	N_5	$(g_{\pi NN})^3/8$

Table 4: Expression of fitting parameters of the phenomenological amplitude in terms of the Lagrangian parameters.

3 Experimental Base

The experimental base for fitting the amplitude parameters was built of the total cross sections in all five channels of the considered reaction in the energy region $P_{\text{Lab}} \leq 500$ MeV/c and the distributions measured in the hydrogen bubble-chamber experiments at these energies [45, 46, 18, 71, 38]. The bubble-chamber data were preferred since they satisfy the condition of the coverage of the reaction phase space in the most complete way (the only restrictions are $P_{\text{proton}} \geq 120$ MeV/c and $P_{\pi} \geq 30$ MeV/c which correspond to 5 mm of the flight distance). The losses occupy only a small part of the phase space (namely, ≤ 2 % in the case of $\{\pi^{-}\pi^{0}p\}$ and ≤ 3 % in the case of $\{\pi^{-}\pi^{+}n\}$ at $P_{\text{beam}} = 400$ MeV/c) and might be easily taken into account during the calculations of theoretical distributions. Besides, the systematic errors of the bubble-chamber experiments are also minimal.

In the course of our fittings we faced the following problem. There are three works in the $\{\pi^{-}\pi^{+}n\}$ channel at close beam momenta:

1. Kirz ($P_{\text{Lab}} = 485$ MeV/c) [46],
2. Blokhintseva ($P_{\text{Lab}} = 457$ MeV/c) [18],
3. Saxon ($P_{\text{Lab}} = 456$ MeV/c) [71].

It was found that results of these works are incompatible. If one tries to describe only distributions from these works without appealing to any other data (total cross sections or other channels' data) then the averaged χ^2 per bin ($\equiv \overline{\chi^2}_{p.b.}$) for distributions by Kirz and Blokhintseva separately and for their sum as well is less than 1. Adding the distributions by Saxon we obtained $\overline{\chi^2}_{p.b.} > 1.5$ for every combinations and even $\overline{\chi^2}_{p.b.} = 2.1$ for the Saxon's distributions themselves.

We should note here, that we have the results of the experiment by Blokhintseva as the collection of events. Hence, we can build any distribution and we did so for all kinds of distributions published in the Saxon's paper. Along with other spectra such distributions also represent the Blokhintseva work [18] in our fittings.

The experiment by Saxon contains more events than the ones by Kirz and Blokhintseva together, so, at first glance, one should prefer to choose his results. However, the processing of films had been performed by the Saxon's group in a quite specific (nontraditional) way. In such films the elastic $\{\pi^{-}p\}$ reaction events look very much like the events of the considered reaction, their total number being ten times greater. To economize manual measurements the group had estimated visually the density of the positive tracks and, basing on the estimate, had selected the events with π^{+} .

However, besides the velocity of the charged particle the density of a track in the bubble chamber depends upon much more another factors like the moment of particle flight relative to the moment of liquid expansion start, the moment of snapshot relative to the moment of particle flight, the liquid superheating degree, etc. This dependence is extremely strong. The above parameters undergo stabilization but the latter never becomes ideal. The rest fluctuations can not prevent the ionization measurements of tracks but for the reliability of the determination of the particle velocity in the every snapshot the control measurements of the bubble density should be performed for the sample track. In the visual estimating the

probability of an error is big especially in the case of the so large number of the processed tracks.

One can estimate the systematic error of the Saxon's work in the following way. The elastic events accidentally selected into the list of the considered reaction anyway will be rejected after measurements by the reaction fit results. The inelastic ones for which the positive track was erroneously identified as the proton one are lost forever. In such a way the statistics become more poor, the parts of the phase space for which the π^+ velocities are small suffering the most significant losses. The measured value of the total cross section is given in the Saxon's work as 1 mbn; since the results of all isotopic analyses of all set of total cross sections data provide the value of 1.4 mbn one can deduce the 30% level of losses of events in the "economizing" routine of the reaction analysis.

So large value of systematic error forced us to withdraw the distributions of the paper [71] from our fittings.

Thus, the distributions liable to treatment belong to three channels of the considered reaction: $\{\pi^-\pi^+n\}$, $\{\pi^-\pi^0p\}$, $\{\pi^+\pi^+n\}$. The data on distributions of works [45], [46], [71], [38] were taken from the journal publications. The major part of distributions of the work [18] has never been published. These are the distributions in the following variables: the squares of invariant masses of all pairs of final particles $W_{\pi^-\pi^+}$, W_{π^-n} , W_{π^+n} , the invariant variables τ , ν_R , ν_I , θ_R , θ_I introduced in [19, 21], the cosine of the angle between the planes determined by CMS momenta of a) the beam and the recoil neutron; b) π^+ and π^- ($\cos\theta_{\pi\pi}$), the cosines of CMS angles of final particles with the beam $\cos\theta_{\pi^-}$, $\cos\theta_{\pi^+}$, $\cos\theta_n$, the angle $D\phi = \phi^- - \phi^+$ of the planes determined by CMS momenta of a) the beam and the π^- meson; b) the beam and the π^+ meson, the azimuth angle ϕ_{beam} and the cosine of the polar angle of the beam $\cos\theta_{\text{beam}}$ in the Saxon reference frame in which the x axis is the direction of the neutron momentum, the z axis being along the vector product of the neutron momentum with the momentum of π^+ meson, $[\mathbf{p}_n, \mathbf{p}_{\pi^+}]$.

The Jones paper (the $\{\pi^-\pi^+n\}$ and $\{\pi^-\pi^0p\}$ channels at $P_{\text{Lab}} = 415$ MeV/c) [38] provides distributions in the squares of invariant masses of all pairs of final particles (namely, $\{\pi^-\pi^+n\}$: $W_{\pi^-\pi^+}$, W_{π^-n} , W_{π^+n} ; $\{\pi^-\pi^0p\}$: $W_{\pi^-\pi^0}$, W_{π^-p} , W_{π^0p}).

The Kirz paper (the $\{\pi^-\pi^+n\}$ channel at $P_{\text{Lab}} = 485$ MeV/c) [46] gives distributions in the invariant masses $W_{\pi^-\pi^+}$, W_{π^-n} , W_{π^+n} of all pairs of final particles and in the cosine of angles of all final particles with the beam in CMS $\cos\theta_{\pi^-}$, $\cos\theta_{\pi^+}$, $\cos\theta_n$.

Another paper by Kirz (the $\{\pi^+\pi^+n\}$ channel at $P_{\text{Lab}} = 477$ MeV/c) [45] contains distributions in the CMS angles of final particles θ_{π^+} , θ_n , the π^+ CMS energy $T_{\pi^+\text{CMS}}$, the momentum P_{π^+} of π^+ in the (π^+, π^+) system and in the nonrelativistic momentum transfer P_{transf} .

One should note that some of these distributions strongly differ from the distribution provided by the empty phase space while there are some with the insignificant difference. This becomes especially clear in terms of (normalized) quasi-amplitudes — see pictures in Figs. 3–8 where almost all distributions are reproduced.

We are using the total cross sections data [3], [4], [5], [6], [7], [9], [15], [16], [17], [18], [25], [26], [28], [38], [41], [42], [43], [45], [46], [48], [49], [53], [64], [66], [71], [72], [76]. 94 points were selected on the grounds of the compatibility analysis of the paper [80] from the total

list of 105 experimental points.

In some variants of fittings (namely, when the theoretical amplitude was not completely real — see the next section where all variants are described in more details) there were used two experimental data points more. These points were fixing the phases of two (nonvanishing at the threshold) isotopic amplitudes by the known values of the elastic P_{31} ($\approx -4^\circ$) and P_{11} ($\approx 2^\circ$) phases in accordance with the final-state interaction theorem.

4 Data Analysis

The analysis of the data described in the previous section required some preliminary steps which are described below. After then we discuss the main results in the subject. 4.2.

4.1 Principal Steps of Analysis

To perform the analysis the following steps had been done:

1. The contributions to the amplitude of every parameter of our model (discussed in the sect. 2) had been calculated analytically according to the Feynman rules of the tree approximation. (The $iM\Gamma$ shifts regularizing the terms with poles located in the physical region were made also for all cross terms to ensure correct crossing properties of the entire amplitude.) The contributions generally come to all 16 scalar–isoscalar form factors defined in eqs. (3), (4); the corresponding expressions had been obtained and transformed to the FORTRAN code with the help of the REDUCE package [35] for analytic calculations in high energy physics.

2. The second step was aimed to simplify the data fitting routine and save a lot of time during thousands of fitting iterations. For a given experimental point (α) the theoretical quantity $\sigma_{(\alpha)}^{\text{Th}}$ confronting the experimental value $\sigma_{(\alpha)}^{\text{Exp}}$ is the integral over the reaction phase space (or over its part in the case of the distribution data) of the squared modulus of the amplitude (10).

Since the set of all parameters $\{A_\nu\}$ including the formal ones enters our amplitude linearly and the conditions for the formal parameters do not contain kinematics we can present the theoretical quantity (12) in the form

$$\sigma_{(\alpha)}^{\text{Th}} = \sum_{\mu,\nu} A_\mu A_\nu C_{(\alpha)}^{\mu\nu}. \quad (31)$$

Then we can build for every experimental point (α) the *correlator* $C_{(\alpha)}^{\mu\nu}$ performing all phase space integrations ones and forever. These calculations had been done for every bin of all distributions with the use of the standard high energy physics package based on the Monte Carlo integration. Since all distributions in question belong to the beam momenta 415, 460, 477, 485 MeV/c few Monte Carlo runs were necessary (and sufficient) to provide the calculations. In the case of the total cross sections the correlator matrix $\hat{C}_{(\alpha)}$ for an experimental point (α) was being recovered during the fittings' run-time by the fast interpolation from 13 fulcrum matrices in every channel precalculated at beam momenta 280, 285, 290, 300, 325,

350, 375, 400, 450, 500, 550, 600 and 650 MeV/c. The calculations of the fulcrum matrices had been performed with the fast and efficient program of Gauss integration described in the paper [24].

3. The content of the third step was the data fittings themselves. Here, we point only the general features and specifics of the approach; more details will be revealed along with the discussion of results.

The fittings had been performed by minimizing the value of χ^2 defined as

$$\chi^2 = \sum_{(\alpha)} \frac{(\sigma_{(\alpha)}^{\text{Th}} - \sigma_{(\alpha)}^{\text{Exp}})^2}{(\Delta\sigma_{(\alpha)}^{\text{Exp}})^2} \quad (32)$$

in the case of the total cross section data. However, to avoid the artificial increase of the statistical weight of the total-cross-section data point for which the numerous distributions also were undergoing fittings we were using the distributions' data $\sigma_{(\alpha)n}^{\text{Exp}}$ which were *normalized* to 1 instead of the total cross section.

The use of the precalculated correlator matrices $\hat{C}_{(\alpha)}$ and the simplicity of the expression (31), being calculated in the course of the iterative minimization of χ^2 , made it possible to perform thousands of fitting runs each of which executing hundreds or even few thousands of iterations. The same specifics of the approach provided the excellent flexibility in respect to variation of both the set of fitting parameters and the set of experimental points. The numerous variants of fittings will be discussed in the next subsection.

4.2 Major Results of Analysis

Already test runs of fitting the distribution data had shown that the simple model of the paper [21] is unlikely to be capable to provide a satisfactory description. Therefore, the first question we were trying to find the answer to was if there exists a relatively simple model consistent with the selected data base (411 experimental points). The answer was “no” and let us now discuss why.

We had been grouping together parameters related to one or another mechanism of the considered reaction since it ought to be a hard task to test $\approx 2^{61}$ variants of all combinations of parameters. There were 7 such groups in total, the largest ones consisting of the sets of the background parameters. Below we are using the following symbolic notations for these groups:

- “b” — parameters of the real background;
- “i” — parameters of the imaginary background;
- “o” — parameters of the OPE contribution;
- “r” — 3 parameters related to the ρ meson;
- “N” — parameters of the nucleon contributions (namely, $\text{SE}_{\pi N}\{N\}$ and $\text{DE}_{\pi N, \pi N}\{N, N\}$ ones);
- “D” — parameters of the Δ contributions (namely, $\text{SE}_{\pi N}\{\Delta\}$, $\text{DE}_{\pi N, \pi N}\{N, \Delta\}$ and $\text{DE}_{\pi N, \pi N}\{\Delta, \Delta\}$ ones);
- “R” — parameters of the N_* contributions (namely, $\text{SE}_{\pi N}\{N_*\}$, $\text{DE}_{\pi N, \pi N}\{N, N_*\}$, $\text{DE}_{\pi N, \pi N}\{N_*, N_*\}$ and $\text{DE}_{\pi N, \pi N}\{N_*, \Delta\}$ ones);

For all possible combinations of the listed groups there had been performed the data fittings with at least 50 random starts. In general, no new solutions had been being revealed after 20–30 starts. In the cases when the number of distinct solutions was greater than usual we had been continuing the search with the increased number of random starts to 100 and more. With one exception this had not provided new solutions (apart the solutions with incomparably large χ^2). Only in the “DRNbior” variant when all groups had been being involved acceptable distinct solutions had been found after 100 starts. The total list of this variant contains 12 solutions, not all of them are shown in the discussed Table. (It should be noted that the latter variant is the most difficult in fitting: the convergence is slow because of huge correlations between parameters, the parameter errors in the gained solutions being too large.) Therefore, we consider the probability of existence of a missed solution to be negligible.

The values of χ^2 of the best solutions are listed in the Table 5. A part of variants is withdrawn there to make the table more compact. The baryon–exchange mechanisms are combined with the sets of parameters “b”, “i”, “o” and “r”. For example, the box in the “DR” row and “bio” column corresponds to “DRbio” variant, etc.; in the column (row) with the empty title we collect the results corresponding to the “pure” mechanism. Initially, the “r” set was considered as a *perturbation* to the basic amplitude since the relatively narrow ρ resonance might get into the reaction phase space at $P_{\text{Lab}} \approx 800$ MeV/c only. (The use of the higher polynomial background in such a role requires to make calculations with about a hundred of the next order terms with free parameters or to find the reasons for rejecting the most of them.) However, the presented values of χ^2 can not provide the inference that the “r” mechanism is unimportant (unless all baryon–exchange mechanisms are committed to action).

It is the examination of the Table 5 which leads to the following conclusions:

1. There is no particle for which a simple exchange mechanism is capable to describe the data.
2. Among the double–particle exchanges the participation of OPE does not look advantageous. (Even the dummy “r” mechanism looks more preferable sometimes.)
3. The leading order ChPT fails to describe the data. (Indeed, all contact terms of Chiral Dynamics and tree–level graphs are contained in the variant “Nbo”; the result of the latter even for parameters being free looks depressing.)
4. The most significant improvement of χ^2 is achieved when the imaginary background “i” is being added; the participation of Δ and N_* exchanges with the strong imaginary part of contributions is leading almost to the same effect.

To make the above general conclusions the knowledge of the absolute χ^2 values was sufficient, especially, since the number of experimental points considerably exceeds the (varying) number of free parameters. For a more subtle deduction one needs an information on χ_{DF}^2 (i.e. χ^2 per degree of freedom). However, before calculating χ_{DF}^2 one first ought to look if there are undetermined and inessential parameters in the solution.

		o	b	bo	bi	bio	bir	bior
		8078.5	6993.9	6799.1	773.28	595.53	598.99	550.87
		9083.8	6996.4	6798.8	854.11	597.10	601.17	556.10
		12115.	6998.0	6800.8			620.91	563.68
			7016.9	6813.2			629.66	570.10
				6823.0				576.84
D	9936.3	987.7	634.49	622.43	546.35	517.90	527.54	491.08
		1105.3	651.55	634.08	546.52	520.18	531.11	493.17
			748.07	644.39	548.19		534.24	
				672.37			544.76	
R	6138.6	1160.2	746.19	618.26	511.88	499.41	468.06	453.23
		1378.3	756.55	636.47	515.07	505.34	484.49	502.90
		3988.6	761.74	638.38		566.52	517.41	523.12
				672.74				
				676.47				
N	13693.	7069.7	6660.6	6649.4	549.83	525.73	513.17	496.87
	13709.	7341.0	6660.8	6649.9	551.27	526.72	515.28	497.00
		7388.9	6668.7	6653.0		527.84	516.82	498.42
		9928.6	6739.4	6674.7		528.84	518.16	500.98
			8508.0	6707.2			518.89	501.18
				6731.2				
D	2758.5	760.88	578.68	564.35	471.09	469.33	448.73	443.09
R		870.24	586.21	566.70	475.71	469.96	466.93	450.85
		978.58	659.71	568.58	483.21	470.86	469.82	
		3544.5		573.63	494.95	479.92	473.89	
						482.53		
D	4438.7	647.74	557.32	550.95	495.19	485.30	473.29	444.11
N	5023.7	793.23	562.20	555.25	496.55	487.58	481.65	463.69
			572.59	561.61	513.20		496.34	
			619.67	574.84				
				576.49				
				609.92				
R	2546.7	907.85	553.01	540.30	467.26	455.12	442.69	426.66
N		1067.6	553.04	568.76	499.38	487.41	486.08	480.20
		2997.9	553.21		519.16	493.38		
			555.16					
			584.36					
D	1430.1	588.65	510.42	506.13	435.72	430.88	426.54	412.84
R	1430.7	710.41	516.79	507.26	449.27	442.20	432.59	418.83
N	1451.5				449.62	443.02	435.85	423.30
					450.10	445.69	447.12	589.75

Table 5: List of χ^2 in distinct solutions obtained from random start (50 tests) with $N_{\text{Exp}} = 411$ experimental points. (In the truncated variant “DRNbior” there are 12 solutions in total obtained in ≈ 500 runs.)

Now we must note the following feature of the discussed results. The numerous solutions in some variants reflect the existence of large correlations of parameters in the variant in question. The estimating of parameter errors by the fitting routine is not then precise enough and our simple algorithm for comparing solutions marks as different the solutions which are, in principle, identical.

To make the situation clear and, what is more important, to reduce the errors of parameters we had performed the series of additional runs eliminating one by one those parameters which relative errors had been being greater than 1 and fitting the data by the rest parameters (while the value of χ_{DF}^2 had been improving). This routine had been applied to all solutions. Unfortunately, there is no enough room to display the results. The Table 6 presents the information on χ_{DF}^2 for some selected variants, the number of parameters in effect N_{P} and the independent lowest $\pi\pi$ scattering lengths. The results of eliminating parameters had no influence on the above conclusions **1.**–**4.** whereas the number of parameters in effect had been considerably reduced. The new inferences derived from the Table 6 read:

5. The considered data base requires a complicated model for its description. Below the level of $\chi_{\text{DF}}^2 < 1.50$ the absolute minimum of the parameter number is 22 (variant “Nbi”); for the most part of the acceptable solutions the number is greater than 30.

6. Assuming the consent that the sequence of signs $+, -, +$ of the $\pi\pi$ scattering lengths $a_0^{I=0}, a_0^{I=2}, a_1^{I=1}$ is *physical*, one finds that a half of all acceptable solutions with the OPE contribution falls to the *unphysical* sector. (The interpretation of the latter phenomenon in terms of threshold values of amplitudes will be discussed in the next section. Here, we simply note that the physical sequence is the one consistent with the predictions of Chiral Dynamics.)

7. The results of fittings can not improve the precision of determinations of $\pi\pi$ scattering lengths. For example, the region $0.06 \leq a_0^{I=0} \leq 0.19$ might be derived from the Table 6 as the preferable one; however, even the current experimental value [30] $a_0^{I=0} = 0.26$ can not be rejected on the ground of the χ_{DF}^2 criterion.

8. The predictions of ChPT in the next-to-leading order [31] $a_0^{I=0} = 0.20, a_0^{I=2} = -0.041, a_1^{I=1} = 0.036, a_2^{I=0} = 0.002$ are compatible with the data base; the separate fittings with the OPE parameters being kept fixed by the above values of scattering lengths, resulted in solutions with the values of χ_{DF}^2 very close to the best ones; for example, in the “DRNbior” variant we get χ_{DF}^2 in the range 1.175 — 1.200.

9. The formal parameters of the imaginary part of the OPE contribution are insignificant at the explored energy region (this is the result of the separate investigations; eliminating these parameters we get some shifts in the parameters of the imaginary background and in the parameters of N_* and Δ isobars, the real parameters of OPE remaining the same).

The discussed above routine of eliminating parameters provided further support of the point **5.**: no one of the considered mechanisms had been rejected as a whole in the course of improving the χ_{DF}^2 value. The listings of this routine contain also a large volume of information about the significance of a given parameter in terms of the “statistical” frequency of its participation. For example, in all variants the parameters A_2, A_3 and A_4 of the linear background of ref. [21] and the parameters A_{13} and A_{15} of eqs. (28), (29) were found to be

	bi		bio					bir		bior				
	χ_{DF}^2	N_{P}	χ_{DF}^2	N_{P}	$a_0^{I=0}$	$a_0^{I=2}$	$a_1^{I=1}$	χ_{DF}^2	N_{P}	χ_{DF}^2	N_{P}	$a_0^{I=0}$	$a_0^{I=2}$	$a_1^{I=1}$
	1.94	26	1.56	30	.04	-.151	-.016	1.58	31	1.46	32	.009	.15	-.040
	1.95	26	1.57	29	.03	-.155	-.011	1.58	32	1.46	32	.014	-.16	.020
								1.64	31	1.50	30	.136	-.12	.048
								1.66	31	1.51	33	.044	-.16	.048
										1.53	33	.045	-.20	.039
D	1.45	33	1.37	24	.16	-.084	.040	1.40	30	1.31	30	.14	-.14	.056
	1.45	25	1.40	30	.11	-.187	.064	1.42	38					
	1.45	27						1.42	36					
								1.44	31					
R	1.35	32	1.33	32	.11	-.004	-.026	1.25	37	1.22	36	.038	.015	.000
	1.36	31	1.33	33	.12	.002	-.025	1.38	37	1.35	39	.073	.0002	.008
			1.51	35	.18	-.138	-.012			1.40	34	.170	-.034	.028
N	1.42	23	1.39	27	.07	.004	-.014	1.36	33	1.32	30	.23	.052	.011
	1.42	22	1.39	28	.07	.004	-.014	1.37	27	1.32	30	.23	-.012	.018
			1.40	33	.16	.026	-.020	1.37	31	1.32	34	.14	-.012	.019
			1.41	28	.16	.023	-.020	1.37	28	1.33	29	.23	.029	.017
								1.37	27	1.33	26	.10	-.014	.015
D	1.25	34	1.25	30	.00	.000	.000	1.20	36	1.21	41	.13	-.026	.046
R	1.27	33	1.26	35	.19	-.058	.038	1.26	40	1.24	46	.12	-.105	.057
	1.29	35	1.26	35	.10	-.048	.033	1.26	39					
	1.33	38	1.31	43	.10	-.016	.026	1.28	38					
			2.01	40	.80	.21	.100							
D	1.31	31	1.29	32	.04	.025	.005	1.27	34	1.19	35	.11	.000	.045
N	1.31	32	1.30	32	.15	-.022	.023	1.29	34	1.24	31	.17	-.104	.048
	1.36	26						1.33	33					
R	1.24	29	1.23	36	.22	.037	-.035	1.19	35	1.15	43	.14	.042	-.008
N	1.34	39	1.31	36	.09	.009	-.015	1.32	45	1.29	40	.18	-.048	.005
	1.39	36	1.32	36	.20	-.047	.0002							
D	1.18	41	1.17	39	.05	-.027	.090	1.16	44	1.14	47	.15	.041	-.026
R	1.20	36	1.19	35	.02	.017	.005	1.18	41	1.15	46	.07	.025	.028
N	1.21	36	1.22	38	.27	.005	.028	1.19	40	1.16	42	.07	-.056	.045
	1.22	37	1.22	38	.05	-.029	.015	1.21	36	1.20	45	.07	-.076	.047
										1.20	41	.17	-.053	.054
										1.21	39	.19	-.059	.053

Table 6: List of χ_{DF}^2 in distinct solutions obtained after deleting undetermined parameters; $N_{\text{Exp}} = 411$ experimental points. (To save the space only the best *unphysical* solutions of the “DRNbior” variant are shown.)

necessary whereas the parameter A_{11} entering the tensor structure of the amplitude \hat{D} had been always ignored. In respect to the OPE parameters the content of the Tables 6, 5 already shows that the parameters are not of the top significance since there are many acceptable solutions without the OPE contribution at all. The parameter g_1 of the paper [21] is found to be relatively important, the D -waves parameters g_2, g_3 being much less necessary.

For illustrations we have chosen the solution from the “DRNbior” variant with $\chi_{\text{DF}}^2 = 1.16$ (see Table 6). The data on total cross sections and the theoretical curves in terms of the quasi-amplitude (15) are drawn in Fig. 2. The most intriguing feature of the discussed curves is expressed by the practical coincidence of the theoretical results for the $\{-0p\}$ and $\{+0p\}$ channels — this is clearly seen from the separate picture in Fig 2 which we draw for the combined data. The picture makes it obvious that the discussed phenomenon is strongly implied by the experimental data. This means that the isotopic amplitude \hat{D} , being the only origin of the difference of the theoretical cross sections of these channels (see eqs. (9)), must vanish indeed.

At Figs. 3–8 one can find the theoretical curves of the same solution for the distribution data discussed in the sect. 3 (in terms of the normalized quasi-amplitude (15)). A part of the data did not enter the fittings — in such cases the curves actually represent our predictions. The normalized quasi-amplitude measures the deviation from the empty-phase-space pattern. In its terms the behavior of the experimental data themselves appears to be quite different.

For example, almost all angular spectra look flat. The explanation is simple: unlike the case of elastic reactions $2 \rightarrow 2$ the 1D distributions are given by the remaining (3-dimensional) phase space integrals in our case of the $2 \rightarrow 3$ process. The averaging over polarizations together with this averaging over the reaction phase space make the angular dependence so weak. However, this can not be true for sections of the phase space and/or for higher dimensional distributions.

In contrast, the distributions in the invariant variables (7) are nontrivial; this proves the choice of variables of the paper [21] to be the characteristic one for the dynamics of the considered reaction.

The results of data analyses described in the current section make it possible to use the obtained amplitude for modeling two other approaches discussed in the Introduction, namely, the one by Olsson and Turner and the Chew–Low extrapolation. What we learn from these tests is discussed in the sect. 5. and 6.

5 Modeling the Olsson–Turner approach

The original idea of the Olsson–Turner approach was to relate the threshold values of the $\pi\pi$ amplitude with the $\pi\pi$ scattering lengths. Therefore, there are two principal steps in the discussed approach: **1)** determination of the threshold limits of amplitudes of the independent isospin channels; **2)** calculation of $\pi\pi$ scattering lengths with the account of other contributions to the above threshold limits.

5.1 Threshold Amplitudes

Let us discuss the first step.

5.1.1 Database

We already know that the threshold amplitudes of 5 experimentally observable channels are not independent. To provide the experimental test of the relations (26) the threshold limits $|M_X^0|$ must be determined from fittings of the data on total cross sections. The results of the similar fittings were already reported starting from publication [27] (see also [67]). The most important conclusion of the work [27] is that the data in the region of $P_{\text{Lab}} \leq 400$ MeV/c admit amplitudes which are linear in the CMS energy. Here, the data up to $P_{\text{Lab}} \leq 500$ MeV/c will be exposed to linear fittings. Moreover, any preliminary selection will be excluded. Indeed, it is the unmotivated preference of one or another set of data which is the reason for contradictory results.

The entire database contains along with the old data (and very old ones) the relatively new results. It should be noted, that before the OMICRON measurements [41]–[44] only the $\{- + n\}$ channel allowed to obtain the definite results of the linear fit; the above mentioned OMICRON data provided the possibility to carry out the procedure also for the $\{- 0 p\}$ and $\{+ + n\}$ channels. The authors of the paper [27] took advantage of the precise data [53] on the $\sigma_{\{00n\}}$ (very close to threshold) and provided the simultaneous linear fit of all channels.

The recent experimental information [66] for the first time makes possible to determine the threshold limit of cross section of the channel $\{+0p\}$ and to test the prediction of the relation

$$M_{\{+0p\}}^0 = M_{\{-0p\}}^0 . \quad (33)$$

(In fact, the approximate equality of cross sections of these two channels is observed along all energy interval considered.)

The separate attention we pay to the $\{+ + n\}$ channel. There are two sets of the near threshold data in the channel $\{+ + n\}$, namely, [43] and [72] which are in certain disagreement. They lead to different threshold limits $|M_{\{+ + n\}}^0|$.

5.1.2 Procedure

Therefore, to provide the definite conclusion four basic variants of fitting were used. Their symbolic notations, entering the summary Table 7, are: ALL — variant with all the data

being included; OMI — in this variant the data [72] are omitted; TRI — variant with the exclusion of the data [43]; X — the variant in which both sets [72] and [43] are excluded. The notation IND is used for the case when the data in each channel are fitted separately (the channel $\{++n\}$ was treated in accordance with the selection adopted in ALL, OMI, TRI and X variants). This helps to understand the trend dictated by data of individual channel in the simultaneous fit.

There were two types of fits in all four basic variants. First, the independent threshold values A^0 and B^0 are treated as being real (or, the same, as obeying the trivial relative phase). We use 7 parameters for simultaneous linear fittings of 5 channels: 2 independent parameters for threshold values (namely, A^0 and B^0) and 5 independent slopes in the invariant kinetic energy

$$T_K = \sqrt{s} - T_0 . \quad (34)$$

(In the course of calculations the latter quantity was taken to be $T_K = \sqrt{(p+k_1)^2} - (m_f + \mu_2 + \mu_3)$ since isospin splitting in the particle masses can not be processed as a correction because of the nonanalytic dependence of the near-threshold phase space on masses — the demonstration can be found in [10].)

Second, we add one parameter to describe the relative phase of the complex quantities A^0 and B^0 .

There is the strong motivation to consider the parameters A^0 and B^0 real. The estimate of the imaginary part of the $\pi 2\pi$ amplitude by the dispersion analysis of the paper [1] allows to consider the amplitude to be approximately real up to the energies $P_{\text{Lab}} = 0.50\text{GeV}/c$. From the general point of view of unitarity relations the value of the imaginary part collects contributions which are due to the following:

a. Three-particle intermediate states. This includes contributions of quasi-two-particle states when the third particle is present as a spectator (namely, N for the $\pi\pi$ state and π for the πN state; the former configuration is characterized by the large imaginary part of isospin-zero $\pi\pi$ amplitude). The three-particle phase space makes this contribution vanish at threshold. (In the paper [11] with the use of $(1/m)$ expansion it was already verified that $\pi\pi$ loops did not contribute to the threshold $\pi 2\pi$ amplitude.)

b. Two-particle intermediate states. In this case only the πN system is allowed. The angular momentum conservation forces these particles to be in the P wave when the final particles at threshold are in the S wave according to Quantum Mechanics — otherwise the P -parity properties of the πN system mismatch those of the $\pi\pi N$ final state. The known phases of the P_{11} and P_{31} waves of the πN -elastic amplitudes approve the neglect of the imaginary part of the $\pi 2\pi$ amplitude at the threshold.

c. Single-particle intermediate states. The only possible one at the threshold of the $\pi 2\pi$ reaction is the Δ isobar. It appears in the P wave of initial particles and its decay into the threshold configuration of the final $\pi\pi N$ state has negligible width [70].

Therefore, there should be no expectations for finding a physically meaningful imaginary part (or a nontrivial relative phase of A^0 and B^0) at the $\pi 2\pi$ threshold. Hence, the threshold identity (25) discussed in the subsect. 2.1. must be practically exact. (The identities (21) are the exact consequences of the isotopic invariance irrespective of the value of the imaginary

part.)

5.1.3 Results

The experimental data are shown in Fig. 9 where the values of quasi-amplitudes $\langle M_X \rangle$ are plotted versus the invariant kinetic energy T_K and the threshold amplitudes $|M_X^0|$ are collected in the Table 7.

This Table is organized in the following way. The first column contains the symbolic name of the selection used for fitting. Five subsequent columns refer to the channel described in the column header. The last column provides the characteristics of the fit — χ_{DF}^2 . To make the comparison easy the additional row IND contains the results of individual fits of every channel (in the case of the $\{++n\}$ channel three additional fits with the exclusion of the controversial data sets, namely [72] and [43], were performed). The last two rows present the predictions of eqs. (25) and (21) based on the data of individual fits of the channels $\{-+n\}$, $\{00n\}$ and $\{-0p\}$.

The bold-face numbers in the boxes ALL, TRI, OMI, X display the results of the solutions in the main fit with $7 = 2+5$ parameters. Every time there was also present another solution of the fit (the slanted numbers in the Table 7 are used for resulting values). It originates from the sign ambiguity which was resolved in part by means of the phenomenological analysis of the subsect. 2.1.3. These auxiliary solutions choose the relation (24) to be true one and it was called *unphysical* since it provides the equal signs of isospin-0 and isospin-2 $\pi\pi$ scattering lengths.

The third line in every box of variants ALL, TRI, OMI, X represents results of the fit with the additional parameter describing the relative phase of amplitudes A^0 and B^0 when A^0 and B^0 are considered as complex numbers. The resulting values of the imaginary parts of the amplitudes $M_{\{-+n\}}^0$ and $M_{\{00n\}}^0$ are given in brackets in the fourth line (the overall phase ambiguity is resolved by assuming the amplitude B^0 to be real).

5.1.4 Discussion

First of all, let us compare the results of the linear fit discussed here with the results of the previous section — it is sufficient to examine the pictures on Figs. 2, 9. One can deduce that the threshold limits provided by the linear fit are good for all channels but the $\{-+n\}$ one. Because of the perceptible curvature revealed by solutions in the latter case the linear fit generally underestimates the value in question.

The Table 7 does not allow to make an unambiguous conclusion on the ground of the quality of the fit only. According to the χ^2 criterion all solutions are practically on equal footing. Even the unphysical ones can not be formally rejected.

The relatively low values of χ^2 of the unphysical solution are, first of all, due to rather large overall uncertainties of experimental data. The more discouraging reason is the existence of arrays of data (almost in every channel) supporting the discussed solution. Only the data of the $\{00n\}$ channel as a whole reject this solution. The examination of the definitions (19) displays that at the value of B^0 being fixed by the data of $\{-0p\}$ and $\{++n\}$

Fit	$\{- + n\}$ $ A^0 + B^0 /\sqrt{2}$	$\{0 0 n\}$ $ A^0 /2$	$\{- 0 p\}$ $ B^0 /2$	$\{+ 0 p\}$ $ B^0 /2$	$\{+ + n\}$ $ B^0 $	χ_{DF}^2
ALL	398 ± 18	413 ± 12	132 ± 6	132 ± 6	264 ± 11	0.99
	524 ± 24	252 ± 12	118 ± 5	118 ± 5	236 ± 11	1.56
	401 ± 150	409 ± 101	132 ± 6	132 ± 6	264 ± 11	1.00
	(74 ± 123)	(52 ± 87)				
TRI	404 ± 18	406 ± 12	121 ± 6	121 ± 6	241 ± 11	0.78
	518 ± 24	260 ± 12	106 ± 6	106 ± 6	212 ± 11	1.33
	406 ± 26	406 ± 18	119 ± 6	119 ± 6	238 ± 12	0.77
	(10 ⁻⁴)	(10 ⁻⁴)				
OMI	372 ± 23	447 ± 13	184 ± 10	184 ± 10	368 ± 20	0.83
	533 ± 32	241 ± 13	136 ± 10	136 ± 10	272 ± 20	1.60
	401 ± 60	410 ± 54	197 ± 11	197 ± 11	395 ± 22	0.80
	(181 ± 23)	(128 ± 16)				
X	387 ± 26	427 ± 14	154 ± 12	154 ± 12	307 ± 24	0.76
	506 ± 36	275 ± 14	83 ± 12	83 ± 12	166 ± 24	1.36
	402 ± 98	410 ± 76	164 ± 14	164 ± 14	329 ± 29	0.76
	(154 ± 40)	(109 ± 28)				
IND	401 ± 19	409 ± 18	155 ± 25	97 ± 51	263 ± 11 237 ± 12 429 ± 26 358 ± 37	ALL TRI OMI X
Eq.(25)	–	–	125 ± 22	125 ± 22	250 ± 44	
Eq.(21)	–	–	–	155 ± 25	310 ± 50	

Table 7: Threshold values provided by data fittings in the variants: ALL — all data; TRI — without [43]; OMI — without [72]; X — excluding [43, 72]. Bold-face numbers correspond to physical solutions of real fits with $7 = 5 + 2$ parameters, slanted ones — to unphysical solutions. The roman font is used for fits with complex amplitudes. The numbers in brackets in the columns of the $\{- + n\}$ and $\{00n\}$ channels display the imaginary part of the resulting amplitude (provided B^0 is real).

channels at the scale no less than $200[\text{GeV}]^{-1}$ the threshold limits of $\{- + n\}$ and $\{0 0 n\}$ channels can not be in balance provided A^0 and B^0 amplitudes are of equal signs. While the closest to threshold points of the OMICRON experiment [43] well agree with the high value of $|M_{\{-+n\}}^0|$ the data of the $\{0 0 n\}$ channel [53] leave no room for describing the cross sections of this channel at so small level (see Table 7).

We end up our discussion of the unphysical solution by noting that there is a striking feature of the entire database: the distribution data, being added to the total cross section ones, did not help to make the distinction between these two kinds of solutions. Moreover, the absolutely best solutions had been found to be the unphysical ones — see Table 6.

In all variants the presence of the imaginary part improves the fit. In the variants ALL and TRI the imaginary part $\text{Im } A^0$ remains consistent with zero: 104 ± 174 — ALL and $10^{-3} \pm 10^2$ — TRI (the amplitude B^0 is considered to be real). In the rest variants the imaginary part is found to be unreasonably large: 255 ± 32 — OMI, 218 ± 57 — X. Nevertheless, it can not help to get rid of the contradiction of data in the $\{- 0 p\}$ and $\{+ + n\}$ channels, especially in the OMI variant of the individual fit.

The examination of the threshold identities (21), (25) clearly displays that the contradiction is between the OMICRON data in $\{- 0 p\}$ and $\{+ + n\}$ channels themselves. Therefore, the analysis of the Table 7 provides the main conclusions that the most consistent from the point of view of threshold identities, the stability against the addition of the complex phase and a reasonable distinction from the unphysical solutions are the threshold amplitudes given in the TRI and ALL variants of the above Table.

5.2 Account of NonOPE Contributions

The discussed above threshold amplitudes are the keystone of the Olsson–Turner approach. (Therefore, it was the inconsistent input of the OMICRON analysis [41]–[44] that provided a controversy in the derived values of $\pi\pi$ scattering lengths.) The original formulae [60] relating the $\pi 2\pi$ threshold amplitudes with the $\pi\pi$ scattering lengths were based — in modern terms — on the leading order Lagrangian of ChPT.

Now the improved formulae take into account the next-to-leading order terms of the Chiral πN Lagrangian [61, 11]. The series of papers [12, 57, 13] deals with various schemes of accounting the above terms in the framework of ChPT and/or Heavy Baryon ChPT and gives the predictions for the nonrelativistic quantities D_1 and D_2 which up to a factor coincide with the discussed above threshold amplitudes A^0 and B^0 :

$$\begin{Bmatrix} D_1 \\ D_2 \end{Bmatrix} = -\frac{\sqrt{\frac{2m}{m+E_0}}}{4m\sqrt{-\tau_0}} \begin{Bmatrix} B^0 \\ A^0 \end{Bmatrix}. \quad (35)$$

The difference in the predicted values (which are quoted in the Table 8 below) makes it paramount to test the approximation schemes of the discussed papers and the hypotheses about the importance of various contributions. The results of our analysis are suitable for this purpose since the phenomenological amplitude determined by fittings is consistent at least with the treated data.

The following Table 8 contains the listing of (nonzero) contributions to the threshold quantities D_1 and D_2 found in the solution with $\chi_{\text{DF}}^2 = 1.16$ (see the variant “DRNbior” of the Table 6 for values of scattering lengths). We also quote here the predictions of papers [12, 57, 13] and the results ALL and TRI of the linear fit from the Table 7 for an easy comparison. The underestimate of the D_2 value by the linear fits ALL and TRI is due to the pointed above tangible departure of the $\{- + n\}$ channel’s solution from the linear pattern.

It should be noted once more that there is no absolute meaning of the separate contributions because of the field redefinition freedom. However, the “on-mass-shell” parameters g_0, g_1, g_2 and g_3 of the 4π vertex are stable and the $\pi\pi$ scattering lengths are well defined in our approach though the “off-shell” contributions of the parameters g_0, g_1, g_2 and g_3 in the Table 8 are model dependent. Hence, the most general inferences which might be derived from this Table are the following:

1. The resulting values of the threshold amplitudes and the quantities D_1 and D_2 are rather small differences of large contributions from various mechanisms.
2. In both quantities the OPE mechanism meets the strong competition from all the rest ones, the Δ being of importance for D_1 while the N_* — for D_2 .
3. Within the overall OPE contribution the influence of the D -wave parameters g_2, g_3 reaches 30% in both quantities D_1 and D_2 .

5.3 Conclusion

We have already seen in the previous subsection that in the experimental side the resolution of an ambiguity in two threshold amplitudes A^0 and B^0 upon which the Olsson–Turner approach is relying is the matter of the precision of experimental data on $\pi 2\pi$ total cross sections. We also noticed the evidence of the inapplicability of the linear fit for the $\{- + n\}$ channel — this enlarges the systematic errors of A^0 and B^0 values. Here, one can see that there are also unknown systematic errors in the theoretical field. To fill in this gap the large amount of experimental and phenomenological information on isobar physics is necessary. Therefore, the approach is losing the advantage of simplicity which had been making it so attractive.

	D_1			D_2		
A_1	310.80	±	35.44	310.80	±	35.44
A_2	194.66	±	6.66	194.66	±	6.66
A_3	531.15	±	13.61	-1062.31	±	27.23
A_4	597.88	±	21.26	1195.77	±	42.52
A_6	-35.15	±	95.36	-35.15	±	95.36
A_{12}	-69.56	±	8.05	-69.56	±	8.05
A_{13}	-312.40	±	7.48	624.80	±	14.96
A_{15}	-159.25	±	4.08	318.50	±	8.17
A_{16}	-186.93	±	16.28	-186.93	±	16.28
A_{17}	-170.52	±	21.80	341.04	±	43.60
o_1	102.14	±	251.12	102.14	±	251.12
o_2	488.02	±	31.38	-976.04	±	62.76
o_3	-101.07	±	33.53	-101.07	±	33.53
o_4	-161.90	±	32.09	323.80	±	64.19
r_2	300.89	±	7.75	-601.78	±	15.50
D_1	-46.75	±	15.48	93.50	±	30.96
D_2	-238.69	±	51.93	42.32	±	55.87
D_3	93.27	±	23.77	-186.54	±	47.53
D_4	-14.91	±	66.48	-115.75	±	133.00
D_5	5.88	±	11.12	-19.53	±	33.28
R_1	52.87	±	108.57	-1079.45	±	192.22
R_3	65.55	±	26.58	-131.09	±	53.15
R_5	0.46	±	12.95	-90.90	±	19.91
R_6	2.41	±	211.45	28.60	±	505.56
R_7	-7.91	±	4.73	-40.14	±	48.72
N_2	128.70	±	32.77	2.81	±	22.75
N_3	152.34	±	45.49	-304.69	±	90.97
N_5	-12.29	±	22.62	15.16	±	21.78
Sum	313.92	±	101.37	-1407.03	±	229.23
[12]	339.69	±	28.63	-1186.96	±	123.64
[57]	344.89	±	31.24	-1179.15	±	136.66
[13]	334.48	±	13.01	-1231.21	±	7.81
ALL	327.78	±	14.90	-1025.54	±	29.80
TRI	300.46	±	14.90	-1008.16	±	29.80

Table 8: Contributions to the values of threshold D_1 and D_2 (in $[\text{GeV}]^{-3}$).

6 Chew–Low Extrapolation

The existence of the pole at $\tau = \mu^2$ in the OPE contribution is the keystone of the Chew–Low approach. However, there are several routines for the extrapolation to this point — the relevant discussion on the applications of the approach might be found in the review paper [50] (see also [58] for a phenomenological introduction); the tests of some variants performed long time ago were reported in the paper [2]. The amplitudes provided by our fits present the possibility to test the approach by modeling the experimental data and to arrive at conclusions which are independent of the finite precision of the input.

6.1 Extrapolation Function

From the very beginning it has become evident that the extrapolation function constructed in terms of the total cross section could not provide a base neither for the linear extrapolation nor for the quadratic one (with the only exception for the case of the $\pi 2\pi$ amplitude build of a *constant* OPE term plus a constant in the same spinor structure S). Therefore, to save the space we discuss only the extrapolation function $F_M(\tau)$ defined in terms of the quasi-amplitude:

$$[F_M(\tau)]^2 \equiv \frac{(\tau - \mu^2)^2}{(-\tau)(2g_{\pi NN})^2} \times \frac{d\sigma(|M|^2)}{d\sigma(1)}. \quad (36)$$

The principal feature of this extrapolation function is the one, reflecting the vanishing of the cross section at $\tau = 0$. It will be commented later on during the discussion of results.

Since — according to the general idea of the Chew–Low extrapolation — only the OPE term of the $\pi 2\pi$ amplitude contributes to the quantity $F_M(\mu^2)$ it is convenient to define the auxiliary function

$$[F_{\text{OPE}}(\tau)]^2 \equiv \frac{(\tau - \mu^2)^2}{(-\tau)(2g_{\pi NN})^2} \times \frac{d\sigma(|M_{\text{OPE}}|^2)}{d\sigma(1)} = \frac{\int_{\Omega(\tau)} \int d\theta_I d\nu_I |V_{4\pi}|^2}{\int_{\Omega(\tau)} \int d\theta_I d\nu_I}. \quad (37)$$

In the above equations both the LHS and the integrals of the RHS depend on the reaction energy s and the dipion invariant mass $s_{\pi\pi}$ which are assumed to be fixed in the course of the extrapolation; the amplitude M_{OPE} is obtained from M by setting to zero all contributions but the OPE one.

The analytic calculation of the function $F_M(\tau)$ is possible only for the case of the simplest models of the amplitude. Therefore, we calculate the function $F_M(\tau)$ obtained in various solutions for our phenomenological amplitude numerically. However, because of the collapse of the integration domain $\Omega(\tau)$ outside the phase space of the $\pi 2\pi$ reaction the numerical calculation of the function $F_M(\tau)$ at $\tau = \mu^2$ also becomes impossible. (The Monte–Carlo based utilities of high energy physics can not generate events outside the phase space for the numerical integration.)

The integration in the RHS of eq. (37) results in the rational function of τ and $s_{\pi\pi}$. Neglecting the imaginary part of the OPE amplitude this function might be cast as the quadratic form in the OPE parameters g_0, g_1, g_2, g_3 of the paper [21]:

$$[F_{\text{OPE}}]^2 = \begin{pmatrix} g_0 \\ g_1 \\ g_2 \\ g_3 \end{pmatrix}^T (\hat{\Phi}) \begin{pmatrix} g_0 \\ g_1 \\ g_2 \\ g_3 \end{pmatrix}, \quad (38)$$

where the upper triangle of the symmetric matrix $\hat{\Phi}$ is explicitly given by

$$\begin{aligned} \Phi_{00} &= 2; \quad \Phi_{01} = \theta_R; \quad \Phi_{02} = 2(9\theta_R^2 + A_1)/9; \quad \Phi_{03} = (9\theta_R^2 - A_1)/9; \\ \Phi_{11} &= (3\theta_R^2 + A_1)/6; \quad \Phi_{12} = (9\theta_R^2 + A_1)\theta_R/9; \quad \Phi_{13} = (9\theta_R^2 - 7A_1)\theta_R/18; \\ \Phi_{22} &= 2(45\theta_R^4 + 10\theta_R^2 A_1 + A_1^2)/45; \quad \Phi_{23} = (45\theta_R^4 - A_1^2)/45; \\ \Phi_{33} &= (45\theta_R^4 + 50\theta_R^2 A_1 + A_1^2)/90; \\ A_1 &= \frac{s_{\pi\pi} - 4\mu^2}{s_{\pi\pi}} [(\theta_R - \tau)^2 - 9s_{\pi\pi}\tau/4]; \quad \theta_R = (\tau + 3\mu^2 - 3s_{\pi\pi})/4. \end{aligned} \quad (39)$$

The discussed function (37) is well defined outside the reaction phase space and at $\tau = \mu^2$ gives the value in question $F_{\text{OPE}}(\mu^2) = F_M(\mu^2)$.

In fact, the actual calculations had been being performed with the function $\tilde{F}_{\text{OPE}}(\tau)$

$$[\tilde{F}_{\text{OPE}}(\tau)]^2 \equiv \int_{s_{\pi\pi} - \Delta s_{\pi\pi}}^{s_{\pi\pi} + \Delta s_{\pi\pi}} ds_{\pi\pi} \sqrt{\frac{s_{\pi\pi} - 4\mu^2}{s_{\pi\pi}}} [F_{\text{OPE}}(\tau)]^2 \bigg/ \int_{s_{\pi\pi} - \Delta s_{\pi\pi}}^{s_{\pi\pi} + \Delta s_{\pi\pi}} ds_{\pi\pi} \sqrt{\frac{s_{\pi\pi} - 4\mu^2}{s_{\pi\pi}}}; \quad (40)$$

since the experimental (and the simulated) data are being presented for a strip $s_{\pi\pi}^{(\alpha)} - \Delta s_{\pi\pi} \leq s_{\pi\pi} \leq s_{\pi\pi}^{(\alpha)} + \Delta s_{\pi\pi}$ in the Chew–Low plot in the $(\tau, s_{\pi\pi})$ variables with the non-negligible width $2\Delta s_{\pi\pi}$. The analytic calculations result in much more complicated expressions than that of eqs. (39), so we do not present the final answers here. Because of the rapid growth of the $\pi\pi$ amplitude with $s_{\pi\pi}$ at the threshold the difference of the simple function (37) with the above one (40) was found to be reaching 20% at $\Delta s_{\pi\pi} = 0.15\mu^2$.

The nonnegligent spread in $s_{\pi\pi}$ has another important issue for the extrapolation. The specific bin (α) is then characterized by the rectangle $(\tau^{(\alpha)} \pm \Delta\tau, s_{\pi\pi}^{(\alpha)} \pm \Delta s_{\pi\pi})$ in the Chew–Low plane $(\tau, s_{\pi\pi})$. The cross section for the bin is given by the integral

$$\sigma_{(\alpha)}(\|M\|^2; \tau) = \int_{s_{\pi\pi}^{(\alpha)} - \Delta s_{\pi\pi}}^{s_{\pi\pi}^{\text{MAX}}} ds_{\pi\pi} R(\|M\|^2; s_{\pi\pi}, \tau), \quad (41)$$

where $R(\|M\|^2; s_{\pi\pi}, \tau)$ stands for the matrix element integrated over the rest 2 variables (which include the $\pi\pi$ scattering angle). The upper limit

$$s_{\pi\pi}^{\text{MAX}} \equiv \text{MAX}\{s_{\pi\pi}^{(\alpha)} + \Delta s_{\pi\pi}, s_{\pi\pi}^+(\tau)\} \quad (42)$$

is independent of τ only for bins (α) for which the strip $s_{\pi\pi}^{(\alpha)} - \Delta s_{\pi\pi} \leq s_{\pi\pi} \leq s_{\pi\pi}^{(\alpha)} + \Delta s_{\pi\pi}$ is going strictly inside the physical domain of the Chew–Low plot. Therefore, in the case of

bins located at the boundaries of the physical interval $[\tau^-(s), \tau^+(s)]$ the physical space in the $s_{\pi\pi}$ variable is bounded not by the value $s_{\pi\pi} + \Delta s_{\pi\pi}$ independent of τ but by the curve

$$s_{\pi\pi}^+(\tau) = \frac{1}{2m^2} \left\{ \tau(s + m^2 - \mu^2) + 2m^2\mu^2 + \sqrt{\tau(\tau - 4m^2)(s - (m + \mu)^2)(s - (m - \mu)^2)} \right\}. \quad (43)$$

As a result, the value of the phase space $\sigma_{(\alpha)}(1; \tau)$ for such bins does depend on τ as well as integrals of powers $(s_{\pi\pi})^n$ do. This makes necessary to withdraw such bins from the extrapolation base regardless of the kind of the extrapolation function. For example, both the cross section $\sigma_{(\alpha)}(\|M\|^2; \tau)$ and the quasi-amplitude have the breaking points at 2 values of τ — at the ones for which $s_{\pi\pi}^+(\tau) = s_{\pi\pi} + \Delta s_{\pi\pi}$. This phenomenon is clearly seen in the Fig. 10. In the course of a practical data treatment the selection of bins is an easy problem which is solved by calculating the empty phase space for the considered array of bins and keeping on the ones with the constant value of the phase space.

Would one know in advance the $s_{\pi\pi}$ dependence of the partially integrated matrix element $R(s_{\pi\pi}, \tau)$ it would be possible to make corrections for the bins intersecting the boundary curve $s_{\pi\pi}^+(\tau)$ and to include more points into the Chew–Low extrapolation. Our curves in Fig. 10 had been corrected by the empty phase space — evidently this is insufficient. (Since our solutions fit well the $s_{\pi\pi}$ distributions which are very distinct from the phase space there are no much room for wondering.) Another possibility to enlarge the base of the extrapolation by cutting more narrow strips in $s_{\pi\pi}$ depends completely on the experimental statistics.

6.2 Simulations of Chew–Low Extrapolation

The statistics of our data (see experimental points in Fig. 10) can not provide a confidence for the results of a real–data extrapolation. Therefore, we were simulating the distributions with the help of the theoretical amplitudes and constructing the extrapolation function $F_M(\tau)$ for a reasonable number of bins. The input data errors then become negligible, hence, the problem might be investigated in its pure state.

Here, we discuss the simulations of τ distributions (for the fixed strip in $s_{\pi\pi}$) performed for several energies, namely, for $P_{\text{Lab}} = 335, 420$ and 460 MeV/c. The extrapolation functions calculated for three types of theoretical amplitudes at $P_{\text{Lab}} = 460$ MeV/c are shown in Fig. 10. The shown data are simulated with the binning and the precision which are only computer–dependent; the same binning of the available experimental data suffers from a lack of statistics — this is clearly demonstrated by the empty experimental bins in the discussed pictures.

The simulated data were subject to extrapolation to the point $\tau = \mu^2$. The true limiting value for each amplitude is being calculated with the use of eq. (40). The linear (*lin*) and the quadratic (*squ*) extrapolation patterns are selected for demonstrations. The results of extrapolations are collected in the Table 9 where the fulcrum numbers of the true limiting values specific for the considered amplitudes are given in the bottom boxes. We display here the variation of the extrapolated values with the choice of the left bound τ_1 , the right bound τ_2 being kept fixed.

The *o* columns of the Table 9 are the undoubted grounds for the crucial inference that even in the simplified case of the pure OPE mechanism the linear extrapolation method

$P_{\text{Lab}} = 335 \text{ MeV}/c, s_{\pi\pi} = 4.15\mu^2$								
n	τ_1/μ^2	τ_2/μ^2	o_{lin}	o_{squ}	g_{lin}	g_{squ}	x_{lin}	x_{squ}
17	-5.519	-1.155	0.6111	0.7889	1.201	0.866	0.1612	0.3578
16	-5.262	-1.155	0.6204	0.7883	1.176	0.909	0.1712	0.3582
14	-4.749	-1.155	0.6382	0.7871	1.138	0.987	0.1898	0.3669
12	-4.235	-1.155	0.6546	0.7892	1.112	1.067	0.2087	0.3723
10	-3.722	-1.155	0.6709	0.7875	1.100	1.140	0.2286	0.3697
8	-3.208	-1.155	0.6858	0.7864	1.099	1.223	0.2479	0.3589
6	-2.695	-1.155	0.6998	0.7906	1.111	1.341	0.2607	0.3953
			0.7870	0.7870	0.6036	0.6036	0.0000	0.0000

$P_{\text{Lab}} = 420 \text{ MeV}/c, s_{\pi\pi} = 4.15\mu^2$								
n	τ_1/μ^2	τ_2/μ^2	o_{lin}	o_{squ}	g_{lin}	g_{squ}	x_{lin}	x_{squ}
17	-10.01	-1.283	0.4497	0.7097	0.4011	0.3829	0.4971	0.5755
16	-9.497	-1.283	0.4672	0.7090	0.3848	0.4435	0.4971	0.5965
14	-8.470	-1.283	0.4999	0.7098	0.3715	0.5568	0.5051	0.6259
12	-7.444	-1.283	0.5315	0.7055	0.3838	0.6502	0.5208	0.6395
10	-6.417	-1.283	0.5598	0.7028	0.4154	0.7361	0.5384	0.6496
8	-5.390	-1.283	0.5845	0.7070	0.4632	0.8261	0.5561	0.6688
6	-4.364	-1.283	0.6089	0.6990	0.5321	0.8703	0.5782	0.6715
			0.7054	0.7054	0.4751	0.4751	0.0000	0.0000

$P_{\text{Lab}} = 460 \text{ MeV}/c, s_{\pi\pi} = 4.45\mu^2$								
n	τ_1/μ^2	τ_2/μ^2	o_{lin}	o_{squ}	g_{lin}	g_{squ}	x_{lin}	x_{squ}
21	-12.58	-1.797	0.1849	0.4911	-0.0071	0.908	0.2755	1.485
20	-12.06	-1.797	0.2015	0.4916	0.0174	1.006	0.3477	1.462
18	-11.04	-1.797	0.2337	0.4917	0.8569	1.200	0.4837	1.405
16	-10.01	-1.797	0.2643	0.4917	0.1830	1.378	0.6084	1.325
14	-8.984	-1.797	0.2928	0.4933	0.3074	1.535	0.7152	1.230
12	-7.957	-1.797	0.3198	0.4951	0.4568	1.658	0.7997	1.131
10	-6.930	-1.797	0.3459	0.4917	0.6242	1.737	0.8584	1.042
8	-5.904	-1.797	0.3695	0.4895	0.8043	1.726	0.8938	0.969
6	-4.877	-1.797	0.3906	0.4939	0.9711	1.653	0.9096	0.922
			0.4886	0.4886	0.3591	0.3591	0.0000	0.0000

Table 9: Results *lin* (*squ*) of the linear (quadratic) Chew–Low extrapolation to the point $\tau = \mu^2$ for the varying left bound τ_1 . The theoretical amplitudes used for data simulations correspond to: *o* — the solution with OPE contribution only; *g* — the solution with all mechanisms; *x* — the solution with all mechanisms excluding OPE. The numbers given in the bottom boxes show the true values at $\tau = \mu^2$.

generally underestimates the value in question and results in the inappropriate systematic error of 25–35%. The impression of some improvement with the shift to the extreme right position of the extrapolation database in the τ interval is misleading since in the conditions of the reduced extrapolation base the effect of nonzero errors of the real experimental data must make the result even more ambiguous. We must also note that the OPE amplitude (i.e., o) does not fit at all the overall data (see Table 5 for values of χ^2). Besides, it was several times pointed out that only the “gauge–covariant” set of contributions makes sense due to the field–redefinition freedom.

In the more realistic case g when all mechanisms are being present (the amplitude g of the solution with $\chi_{\text{DF}}^2 \approx 1.16$ is at least compatible with the overall database) there are no advantages in both the linear and the quadratic extrapolation methods; the coincidence of the results with the exact answers seems to be of a random nature. The 200–300% deviation makes it unreliable to use both the linear and the quadratic extrapolations even for estimations.

What is really disappointing it is the examination of the columns x . The nontrivial answers in this case raise suspicions that the extrapolations follow the dictate of the experimental data rather than the theoretical amplitude. Indeed, the theoretical amplitude x fits well the data but *it has no pole at $\tau = \mu^2$ at all!*

6.3 Discussion

In view of the negative general conclusion on the applicability of the Chew–Low extrapolation approach at the considered energies we need to shed more light on its origin.

The separate clarification is necessary for the case of the pure OPE mechanism since the application of the Chew–Low approach is based on the hypothesis of the OPE dominance. Indeed, if the nature follows the simplest pattern of the OPE dominance in the $\pi 2\pi$ reaction then 6–8 data points are enough for successful extrapolation — the small discrepancy displayed in the Table 9 (which must be growing with the energy) is due to different accounting of isospin breaking in the main program and in the extrapolation function (40).

It is not so difficult to realize that the small departure of the extrapolation function (37) from the linear pattern is solely due to the participation of the D –wave parameters g_2 and g_3 — see the quantities Φ_{22} , Φ_{23} , Φ_{33} given by eqs. (39). In the absence of the latter the internal integrations of the leading order ChPT amplitude in the formula (37) result in the linear function of τ . At the considered energies the influence of the quoted parameters on the $\pi\pi$ amplitude itself is negligible. The deviation of the extrapolation function from the linear shape is small but its effect on the results of extrapolations is found to be drastic.

The off–shell appearance of the $\pi\pi$ amplitude in the $\pi 2\pi$ reaction acts the part of the magnification lens in respect to D –wave parameters — we have already seen this in the previous section when discussing their contributions to the threshold amplitudes. However, the above phenomenon does not present an obstacle by itself since the quadratic extrapolation for a pure OPE amplitude is proved to be exact and stable.

It is the complicated form of the $\pi 2\pi$ amplitude revealed by our data fittings which rules out the possibility of a reliable application of the Chew–Low extrapolation in the simplest

manner. This conclusion is derived in terms of a particular ansatz of the extrapolation function (36). Let us now discuss why the conclusion is of more general nature.

There is the difference of our function $F_M(\tau)$ with the ones defined in terms of cross sections — we are extracting the square root of the eq. (36). The results of the extrapolation of the square of the function $F_M(\tau)$ in terms of the ansatz

$$[F_M(\tau)]^2 = [F_0 + F_1(\tau - \mu^2) + F_2(\tau - \mu^2)^2]^2 \quad (44)$$

are completely equivalent to the ones displayed in the Table 9. At the same time the extrapolation via

$$[F_M(\tau)]^2 = \tilde{F}_0 + \tilde{F}_1(\tau - \mu^2) + \tilde{F}_2(\tau - \mu^2)^2 \quad (45)$$

provides worse results.

Hence, we see no reason in keeping on the cross-section form. It is not the point which is capable to disapprove our conclusions. So let us discuss another feature which is implemented into our extrapolation function (36).

There is the property of the pure OPE cross section $\sigma_{|\tau \rightarrow 0} = 0$ which was displayed long time ago as by the nonrelativistic calculations (see, for example the textbook by Källén [39]) as well as by the relativistic ones (like that of the paper [58] by Naisse and Reignier). The work [2] by Baton, Laurens and Reignier provided the phenomenological test of this property by the high energy ($P_{\text{Lab}} = 2.77 \text{ GeV}/c$) data — since then it was being built into the applications of the Chew–Low procedure as a standard feature. Nevertheless, the known failures of applications of the Chew–Low approach were associated with the relying on the very property we are discussing here — see the review [50] by Leksin. The more close analysis shows that in some cases the foothold on the property $\sigma_{|\tau \rightarrow 0} = 0$ in the definition (36) is the reason of overshooting of the quadratic extrapolations which are accurately following the extrapolated data in the physical region.

Let us now briefly remind what is the theoretical status of the hypothesis that $\sigma_{|\tau \rightarrow 0} = 0$. Definitely, it is the exact property of the pure OPE mechanism. What the value of the matrix element $\langle \pi_2 \pi_3 N(q) | S | \pi_1 N(p) \rangle$ at $p = q$ is in the general case is the kinematical problem in part. (It should be noted that the point for which $p = q$ is located outside the physical region both for the $\pi N \rightarrow \pi \pi N$ reaction and for the 4π vertex since the condition $p = q$ implies $s_{\pi\pi} = \mu^2$.)

The S structure of the amplitude (10) gets the same multiplier $(-\tau)$ in the unpolarized matrix element (13) as the OPE contribution does. This structure gives rise to spin–flip amplitudes which are the only amplitudes of the considered reaction surviving at the threshold. However, besides this spinor structure there are three more; kinematically, their contributions to the quantity (13) are determined by the matrix (14).

Thus, to make the matrix element (13) vanish at $p = q$ all entries of the matrix (14) must become zero simultaneously. The analysis of the explicit expressions (for which we have no room here) shows that three conditions are necessary: 1) $s = (m + \sqrt{s_{\pi\pi}})^2$; 2) collinear final pions $k_2 = k_3$; 3) Chiral limit $\mu = 0$. The last condition is also the only general reason to make the considered structures vanish dynamically.

Therefore, in the real dynamics the quantity $\|M\|_{\tau \rightarrow 0}^2 (\sigma(\tau = 0))$ stands for expressing the Chiral symmetry breaking which is similar to the πN -elastic Σ term. It depends on the energy but seems to be rather small. Nevertheless, it prevents to make the safe *simplification* in the definition of the extrapolation function, namely, to divide the quasi-amplitude by $\sqrt{-\tau}$ in our case. Thus, we arrive at the conclusion that, from one side, the complicated dependence of the physical amplitude on τ makes useless the linear and the quadratic extrapolation methods even in terms of the quasi-amplitude, from the other side — the presence of the Chiral symmetry breaking in the true amplitude forbids to soften the dependence in the extrapolation ansatz.

6.4 Remark on D -Wave Parameters

The parameters g_2, g_3 of the cross-symmetric ansatz of the $\pi\pi$ amplitude (see [20], [21], [23]) determine the values of the D -wave scattering lengths, therefore, we call them the D -wave parameters here. Because of the crossing symmetry the same D -wave parameters determine also the slopes of the S -wave amplitudes (see eqs. (59), (60) of the ref. [21] and eqs. (73)–(104) of the ref. [23]).

Due to the considerable growth of the $I = 0$ amplitude the contribution of the slopes to the integrated over $s_{\pi\pi}$ cross section (extrapolated by the Chew–Low method) appears to be large.

This very phenomenon makes it possible to extract the discussed parameters from the near-threshold $\pi 2\pi$ experiment, otherwise it is simple to verify that at the considered energies the contribution to the $\pi\pi$ and $\pi 2\pi$ cross sections by the D waves themselves is negligible. This also presents the additional motivation for the careful handling of the crossing properties of the amplitudes of $\pi\pi$ and $\pi N \rightarrow \pi\pi N$ reactions.

7 Conclusions

Throughout the paper we were making the inferable statements along the discussions. Here, we remind the most important ones and develop the general conclusions.

7.1 Data

Our present work is devoted to the analysis of the near-threshold data on the $\pi 2\pi$ reaction. The data base described in sect. 3. consists of the experimental total cross sections and 1-dimensional distributions. The full-kinematics data of the work [17] also had been presented in the same form. This needs some comments.

The available 1023 full-kinematics events of the quoted work constitute the solid ground for the total cross section; 10–14 bins of a 1-dimensional distribution have a good filling with the averaged number of 60–100 events per bin; the filling of 8×8 bins of a 2-dimensional distribution is satisfactory (15 events per bin in the average) while the filling of $6 \times 6 \times 6$ of the 3-dimensional ones and $4 \times 4 \times 4 \times 4$ of the 4-dimensional bins is poor. In this conditions of

the difficult choice between the poor filling of bins and the loss of the kinematical information we formed multiple 1–dimensional projections for the data to bring to light the behavior in the crucial variables.

We created some additional 1D projections of the data [17] and tested them with the obtained solutions — the description was found to be excellent.

The use of the numerous lower dimensional distributions acts the part of a kind of the tomography method. The fittings showed that at a distance from resonance poles this works. The improved statistics of the contemporary experiment [74, 75, 40, 73] definitely must make the direct use of the full–kinematics data more preferable.

The general properties of the treated data base are found to be:

1. The precision of data is insufficient to improve the accuracy of the determination of characteristics of the $\pi\pi$ scattering. However, this is the problem not only of the data.

2. The coverage of the behavior of the low energy amplitude is good; practically, there were no losses of convergence in the course of fittings. The numerous solutions reflect the complexity of the reaction amplitude — the current experimental setup can not be charged for this (we shall continue this discussion below in the subsects. 7.2., 7.3.).

3. The distribution data of the $\{++n\}$ channel are found to be extremely important for the resolution of parameter correlations. In the absence of these data the convergence of fittings becomes tremendously slow, the number of iterations being increased by several orders.

To resume we state that the considered data base is in principle sufficient for determination of the phenomenological near–threshold $\pi 2\pi$ amplitude. Certainly, the need in the better quality of data in respect to the precision of the obtained parameters and the multiplicity of solutions is obvious. First, the quality of the newest data will be much better and, second, it seems oversimplified to charge only the data with this problem. The more detailed discussion of its origin will be given in the next subsection.

7.2 Amplitude and Major Results

Our amplitude is built on the rather conservative basis. However, the orientation towards the modern ChPT approach in constructing the model might be lacking of an intrinsic tool for making the right explanation, if failed, whether an inconsistency of data or the neglect of higher order terms are responsible for the inappropriate fit. If successful, the approach provides the only conclusion that at the considered order ChPT is compatible with data — a substantial estimate of the systematic error of determination of the low energy constants is impossible.

The approach of HBChPT deserves the separate remark. Unlike the case of the πN –elastic scattering this approach is, probably, inapplicable to the case of the $\pi N \rightarrow \pi\pi N$ reaction considered here. One should remind the basic keystones of HBChPT: 1. Nonrelativistic limit; 2. Small–pion–momentum expansion; 3. Heavy baryon approximation. Then, let us consider the identity

$$\bar{u}(q)(\hat{k}_1 - \hat{k}_2 - \hat{k}_3)i\gamma_5 u(p) = -2m \bar{u}(q)i\gamma_5 u(p) , \quad (46)$$

which is specific to the relativistic form of the $\pi 2\pi$ amplitude. The identity can not support the above points 2., 3. simultaneously.

In the present paper we consider the amplitude of the $\pi 2\pi$ reaction built of numerous resonance contributions (including the separately treated OPE mechanism) and the smooth polynomial background (see sect. 2.). Its complicated appearance reflects the influence of the (generally, off-shell) processes like $\pi\pi \rightarrow \pi\pi$, $\pi N \rightarrow \pi N$, $\pi N \rightarrow \pi N_*$, $\pi N \rightarrow \pi\Delta$ on the near-threshold region of the discussed reaction.

The fittings strongly confirmed the importance of all quoted exchange mechanisms. This result can not be considered as the totally new one. For example, the importance of isobars already had been stressed in the paper [37] in terms of the sophisticated analysis of the amplitude form.

The near-threshold region $280 \leq P_{\text{Lab}} \leq 500$ MeV/c can not be considered as the selfcontained one because of large Δ , N_* widths. The isobars extend their strong influence up to the very $\pi 2\pi$ threshold (this is demonstrated by the Table 8). In the absence of isobar contributions the considerable improvement of the fit due to the imaginary background serves as an indirect evidence of the importance of the discussed isobar mechanisms (see Table 5). The interrelation of these mechanisms with the OPE one will be discussed below.

In view of the discussion of the role of background parameters (see subsect. 2.4.) it is not so surprising that only few of them are found important in the fittings when all exchange mechanisms are being present. The fact that the parameters of the isospin amplitude D are found to be consistent with zero reflects the negligible influence of higher τ -resonances (like $SE_{NN}(\omega)$) on the amplitude in the considered energy region. Even the nonzero contributions to this isospin amplitude from isobar exchanges almost cancel each other — this might be derived from an approximate equality of the resulting theoretical cross sections of $\{-0p\}$ and $\{+0p\}$ channels.

The OPE contribution is in the center of our investigations. In all variants the improvement of χ_{DF}^2 with the inclusion of OPE is found to be statistically important (see Tables 5, 6). The 4π vertex of the OPE graph is taken in the direct amplitude form which contains 4 parameters g_0 , g_1 , g_2 and g_3 and respects the isospin, crossing and approximate-unitarity properties of the $\pi\pi$ amplitude off the mass shell. In terms of the $\pi\pi$ -scattering lengths the values of these parameters in the best physical solutions are:

χ_{DF}^2	$a_0^{I=0}$	$a_0^{I=2}$	$a_1^{I=1}$	$a_2^{I=0}$	$a_2^{I=2}$
1.161	0.07 ± 0.12	-0.056 ± 0.036	0.045 ± 0.017	0.0052 ± 0.0031	-0.0005 ± 0.0014
1.203	0.07 ± 0.11	-0.076 ± 0.073	0.047 ± 0.025	0.0023 ± 0.0027	-0.0013 ± 0.0014
1.205	0.17 ± 0.12	-0.053 ± 0.039	0.054 ± 0.022	0.0054 ± 0.0025	-0.0002 ± 0.0012
1.212	0.19 ± 0.11	-0.059 ± 0.045	0.053 ± 0.022	0.0062 ± 0.0027	0.0006 ± 0.0015
[30]	0.26 ± 0.05	-0.028 ± 0.012	0.038 ± 0.002	0.0017 ± 0.0003	0.0001 ± 0.0003

Here, we list also the currently adopted experimental values of the compilation [30].

Generally, the solutions display that the precision of determination of the D -wave parameters g_2 and g_3 is not worse than that of g_0 , g_1 parameters. This was attributed to the characteristic energy dependence of the isospin-zero S wave (see subsect. 6.4.). The parameters of the latter via crossing and kinematics are connected to D -wave scattering lengths

— this is clearly demonstrated by the $a_2^{I=0}$ errors in the above list.

The poor precision of determination of the $\pi\pi$ -interaction parameters has its origin in 3 principal reasons: 1) the data accuracy; 2) the competition of other (nonOPE) mechanisms; 3) the incomplete nature of the current experimental setup.

The first point is evident — the data accuracy will be improved soon (look [68] for the survey of experiments).

The second one stems mainly from the isobar exchanges — this is clearly revealed by fittings: whenever an isobar mechanism is absent it is easy to find a solution with $a_0^{I=0}$ in the range 0.20 — 0.30; it drops to the 0.00 — 0.20 range if all isobar mechanisms are involved (it is interesting that the effect of ρ exchanges is quite opposite). In other words, the larger values of $\pi\pi$ -scattering lengths are gained when OPE is forced to stay for an essential but missed isobar contribution.

The important question is about the nature of parameters which correlations with the OPE set g_0, g_1, g_2, g_3 are so devastating. Unfortunately, these are not the parameters of the DE-type graphs which might be estimated from the decay characteristics or might be known (like the $g_{\pi NN}$ constant) from the low-energy πN phenomenology. Instead, the root correlations are due to parameters R_1 – R_4 and D_1 – D_4 of the $SE_{\pi N}(N_*)$, $SE_{\pi N}(\Delta)$ graphs (see Tables 4, 2, 3). The explanation is simple. Parameters of the graphs of the SE type play the same role in respect to the ones of the DE type as the background parameters A_1 – A_{18} (and their analogs i_{19} – i_{36}) do in respect to all exchange parameters. Indeed, outside the resonance region the contraction of any pole in the DE graph leads to the single-pole contribution, i.e. to the one described by the SE graphs.

Here, one observes the interrelation of the point 2. with the first one since the data restricted to the region below resonances can not help much to fix up parameters of processes like $\pi N \rightarrow \pi N_*$, $N_* \rightarrow \pi\pi N$, $\pi N \rightarrow \pi\Delta$, etc.

We found the numerous set of solutions describing the data at the acceptable level of χ^2 . The origin of this phenomenon must be explained in part by the importance of all 4 spin structures of the $\pi 2\pi$ amplitude (see eqs. (4), (10)). This is the reason number 3 for the poor accuracy of our final results.

Indeed, the unpolarized data measure only one combination of spin structures (namely, the combination given by the matrix element (13)) leaving them almost free to stand one for another. Therefore, the absence of polarized measurements in the energy region $P_{\text{Lab}} \approx 500$ MeV/c and the abundance of mechanisms specific to the considered reaction is the reason of huge correlations of OPE parameters with the rest ones on the available data base.

Meanwhile, the extreme importance of the nucleon spin in the considered reaction at higher energies had been recently reported by Svec in the paper [79]. In the results of our analysis and modeling the Chew–Low extrapolation function we see the clear signal of nontrivial spinor structures. This claims for the polarization measurements of $\pi N \rightarrow \pi\pi N$ reactions at the discussed energies. Up to now the known polarization measurements of the $\pi 2\pi$ reactions had been performed at considerably higher energies, for example, at 5.98 GeV/c and 11.85 GeV/c [51] and at 17.2 GeV/c [34]. Their analyses [78], [8] already proved such measurements to be detailed sources of information on the $\pi\pi$ interaction (at high energies).

Certainly, the complete polarization experiment requires the analysis of the polarization of the final nucleon — in the near future this is hardly to be carried out for such rare processes as the considered one. Nevertheless, the examination of the spinor structure of the considered amplitude (4) displays that the almost exhaustive information might be obtained already from the experiment with the polarized target. Indeed, there are two independent asymmetries

$$A_{\pm}(\mathbf{s}) = \frac{\sigma(\mathbf{s}; \mathbf{k}_{\pm}^{\perp}) - \sigma(\mathbf{s}; -\mathbf{k}_{\pm}^{\perp})}{\sigma(\mathbf{s}; \mathbf{k}_{\pm}^{\perp}) + \sigma(\mathbf{s}; -\mathbf{k}_{\pm}^{\perp})}, \quad (47)$$

where \mathbf{s} is the vector of the nucleon polarization and \mathbf{k}_{\pm}^{\perp} are the projections of vectors $\mathbf{k}_{\pm} = \mathbf{k}_2 \pm \mathbf{k}_3$ to the plane which is orthogonal to \mathbf{s} . Their measurements must provide an information on two additional combinations of four spinor structures of the decomposition (4) which are independent from the combination of the matrix element (13).

7.3 General Conclusion

In view of the results of modeling the Chew–Low extrapolation and the Olsson–Turner approach we conclude that only the approach based on the extensive phenomenological model (*a la* Vicente–Vacas) can help in investigations of the considered reaction. The investigations require to develop the common analyses of related processes like $\pi N \rightarrow \pi N_*$, $\pi N \rightarrow \pi \Delta$ — i.e. the processes described by the Lagrangian terms listed in Tables 2, 3 — and, hence, to extend the energy region up to $P_{\text{Lab}} \sim 1 \text{ GeV}/c$. In other words, the problem of determination of the low–energy $\pi\pi$ –scattering characteristics is a part of the more comprehensive problem of investigation of $\pi 2\pi$ dynamics at low and intermediate energies.

The results of contemporary experiments [40, 73, 74] must provide much more precise determination of $\pi\pi$ parameters since their correlations with the unknown parameters of isobar mechanisms originating from the discussed above spin structures will be resolved in part due to the improved data accuracy. In this respect the role of the polarized data is difficult to over–estimate.

The amplitude which structure will be fixed by the analysis of statistically significant data might gain the wide range of applications beyond the testing of ChPT predictions. For example, it might be used for the common analysis of $\pi N \rightarrow \pi\pi N$, $\gamma N \rightarrow \pi\pi N$ and πN –elastic data, for investigations of the η production in the process $\pi N \rightarrow \eta N$, for correcting experimental distributions obtained at devices with the restricted geometry and for other investigations at intermediate energies. This is ensured by the fundamental role of the $\pi N \rightarrow \pi\pi N$ reaction in nuclear and particle physics.

8 Acknowledgments

This research was supported in part by the RFBR grant N 95-02-05574a. We thank T.A. Bolokhov, P.A. Bolokhov, V.A. Guzey, A.N. Manashov, V.V. Vereshagin V.L. Yudichev, A.Yu. Zakharov for checking the formulae, testing the code and for other help at various stages of the project. We are grateful to P. Amaudruz, A. Bernstein, F. Bonutti, J. Brack, P. Camerini, G.A. Feofilov, E. Frlež, N. Grion, G. Hofman, R.R. Johnson, M. Kermani, M.G. Olsson, O.O. Patarakin, D. Počanić, R. Rui, M. Sevier, G.R. Smith for helpful discussions. We especially thank the CHAOS team for presenting computer powers of ALPHA stations at TRIUMF (Vancouver) and INFN (Trieste).

References

- [1] I.J.R. Aitchison, J.J. Brehm. Phys. Lett., **84B** (1979) 349–353.
- [2] J.P. Baton, G. Laurens and J. Reignier. Nucl. Phys. **B3** (1967) 349.
- [3] B.C. Barish R.J. Kurz et al. Phys. Rev. **135B** (1964) 416.
- [4] Yu.A. Batusov, C.A. Buniatov et al. JETP /Russian/ **40** (1961) 1528.
- [5] Yu.A. Batusov, C.A. Buniatov et al. YaF /Russian/ **1** (1965) 562, 687.
- [6] Yu.A. Batusov, C.A. Buniatov et al. YaF /Russian/ **18** (1973) 86.
- [7] Yu.A. Batusov, C.A. Buniatov et al. YaF /Russian/ **21** (1975) 308.
- [8] H. Becker, et al. Nucl. Phys. **B151** (1979) 46.
- [9] A.A. Belkov, C.A. Buniatov et al. YaF /Russian/ **31** (1980) 181.
- [10] J. Beringer. πN -Newsletter, **7** (1992) 33, issn 0942–4148.
- [11] V. Bernard, N. Kaiser and Ulf-G. Meißner. Phys. Lett. **B332** (1994) 415; **B338** (1994) 520.
- [12] V. Bernard, N. Kaiser and Ulf-G. Meißner. Nucl. Phys. **B457** (1995) 147.
- [13] V. Bernard, N. Kaiser and Ulf-G. Meißner. *The Reaction $\pi N \rightarrow \pi\pi N$ above Threshold in Chiral Perturbation Theory*. Preprint KFA-IKP(TH)-1997-05, Mar. 1997, 29p.; hep-ph/9703218.
- [14] J. Bijenes, G. Colangelo, G. Ecker, J. Gasser and M.A. Sainio. Phys. Lett. **B374** (1996) 210.
- [15] S.W. Bjork, S.E. Jones et al. Phys. Rev. Lett. **44** (1980) 62-65 .
- [16] I.M. Blair, H. Muller, G. Torelli, E. Zavattini. Physics Lett. **32B** (1970) 528-532.

- [17] T.D. Blokhintseva, V.G. Grebinnik et al. JETP, **44** (1963) 498.
- [18] T.D. Blokhintseva, A.V. Kravtsov et al. YaF **12** (1970) 101-108 /Russian/, Sov. Journ. Nucl. Phys, **12** (1971) 55-61 /English/.
- [19] A.A. Bolokhov, V.V. Vereshchagin and S.G. Sherman. Yad. Fiz., 45, 508–513, 1987; Sov. J. Nucl. Phys. **45** (1987) 319–322.
- [20] A.A. Bolokhov, S.G. Sherman, V.V. Vereshagin. Yad. Fiz. **46** (1987) 585.
- [21] A.A. Bolokhov, V.V. Vereshagin and S.G. Sherman. Nucl. Phys. **A530** (1991) 660.
- [22] A.A. Bolokhov and M.E. Sevier. Interpretation of $\pi N \rightarrow \pi\pi N$ measurements. *in* A.M. Bernstein and B.R. Holstein (eds.), Chiral Dynamics: Theory and Experiment, Proceedings of the Workshop held at MIT, Cambridge, MA, USA, 25–29 July 1994, Lecture Notes in Physics, LNP 452 (Springer–Verlag, Berlin and Heidelberg, 1995), p. 115.
- [23] A.A. Bolokhov, et al. *Cross-Symmetric Expansion of $\pi\pi$ Amplitude Near Threshold*. Submitted to Yad. Phys. (1997).
- [24] A.A. Bolokhov, P.A. Bolokhov, T.A. Bolokhov and S.G. Sherman. “Gauss Integration over Relativistic 3–Body Phase Space for 1–Dimensional Distributions of $2 \rightarrow 3$ Reaction”, preprint hep-ph/9601264; SPbU-IP-96-1, Sankt-Petersburg (1996) 32p.
- [25] C.A. Buniatov, V. Kurbatov, et al. Nucl. Phys. **42B** (1972) 77-84.
- [26] C.A. Buniatov, G.V. Jolobov, et al. Sov. Nucl. Phys./Russian/ **25** (1977) 325-334.
- [27] H. Burkhardt and J. Lowe. Phys. Rev. Lett. **67** (1991) 2622
- [28] J. Deahl, M. Derrick, et al. Phys. Rev. **124** (1961) 1987-1994 .
- [29] J.F. Donoghue, E. Golowich and B. Holstein. Dynamics of the Standard Model. Cambridge University Press, NY, 1992.
- [30] O. Dumbrais, et al. Nucl. Phys. **B216** (1983) 277.
- [31] J. Gasser and H. Leutwyler. Phys. Lett. **125B** (1982) 312; Phys. Lett. **125B** (1982) 325.
- [32] J. Gasser and H. Leutwyler. Ann. Phys. (NY) **158** (1984) 142; Nucl. Phys. **B250** (1985) 465, 517, 539.
- [33] C.J. Goebel. Phys. Rev. Lett. **1**, (1958) 337; G.F. Chew and F.E. Low. Phys. Rev. **113** (1959) 1640.
- [34] G. Grayer, et al. Nucl. Phys. **B75** (1974) 189.

- [35] A.C. Hern. REDUCE User's Manual. Rand Corp., Santa Monica. 1985.
- [36] G. Höhler. *Pion-Nucleon Scattering*. Landolt-Börnstein, New Series, ed. Schopper, Vol. I/9 b2 (Springer-Verlag, 1983).
- [37] R.R. Johnson, N. Fasel and N. Suen. πN -Newsletter **8** (1993) 121.
- [38] J.A. Jones, W.W.M. Allison, D.H. Saxon. Nucl. Phys. **B83** (1974) 93-107.
- [39] G. Källen. *Elementary Particle Physics*. Addison-Wesley Publishing company, Inc., Reading, Massachusetts, Palo Alto, London., 1964.
- [40] M.A. Kermani. First results of exclusive measurements of $\pi N \rightarrow \pi\pi N$ with CHAOS detector. in A.M. Bernstein and B.R. Holstein (eds.), Chiral Dynamics: Theory and Experiment, Proceedings of the Workshop held at MIT, Cambridge, MA, USA, 25-29 July 1994, Lecture Notes in Physics, LNP 452 (Springer-Verlag, Berlin and Heidelberg, 1995), p. 115.
- [41] G. Kernel, D. Korbar et al. Phys. Lett., **B216** (1989) 244-248.
- [42] G. Kernel, D. Korbar et al. Phys. Lett., **B225** (1989) 198-202.
- [43] G. Kernel, D. Korbar, et al. Z. Phys. **C48** (1990) 201.
- [44] G. Kernel, et al. OMICRON. Z. Phys. **C51** (1991) 377.
- [45] J. Kirz, J. Schwartz, R.D. Tripp. Phys. Rev. **126** (1962) 763-765.
- [46] J. Kirz, J. Schwartz, R.D. Tripp. Phys. Rev. **130** (1963) 2481-2484.
- [47] M. Knecht, B. Moussalam, J. Stern and N.H. Fuchs. Nucl. Phys. **B457** (1995) 513.
- [48] A.V. Kravtsov, L.L. Nemenov, et al. YaF **20** (1974) 942 /Russian/.
- [49] A.V. Kravtsov, E.A. Lobachov, et al. Nucl. Phys. **B134** (1978) 413.
- [50] G.A. Leksin. Uspekhi., **102**, 387-430, 1970.
- [51] A.de Lesquen, et al. Phys. Rev. **D32** (1985) 21.
- [52] H. Leutwyler. "On the Foundations of Chiral Perturbation Theory", preprint Univ. of Bern. BUTP-93/24; "Masses of the Light Quarks", preprint Univ. of Bern. BUTP-94/8; "Principles of Chiral Perturbation Theory", preprint Univ. of Bern. BUTP-94/13; "Goldstone Bosons", preprint Univ. of Bern. BUTP-94/17; "Foundations and Scope of Chiral Perturbation Theory", preprint Univ. of Bern. BUTP-94/18.
- [53] J. Lowe, B. Bassalleck, et al. Phys. Rev. **C44** (1991) 956-965.
- [54] D.M. Manley. Phys. Rev., **D30** (1984) 536.

- [55] B.R. Martin, D. Morgan and G. Shaw. Pion–Pion Interactions in Particle Physics. Academic Press, NY, 1976.
- [56] Ulf–G. Meißner. Rep. Prog. Phys. **56** (1993) 903.
- [57] Ulf–G. Meißner. *The Reaction $\pi N \rightarrow \pi\pi N$ at Threshold*. Talk given at 7th International Conference on the Structure of Baryons, Santa Fe, NM, 3–7 Oct. 1995. Preprint TK 95 29 (1995) 4p.; hep-ph/9510390.
- [58] J. Naisse and J. Reignier. Fortschritte der Physik **12** (1964) 523.
- [59] L.M. Nath, B. Estemadi and J.D. Kimel. Phys. Rev. **D3** (1970) 2153.
- [60] M.G. Olsson and L. Turner. Phys. Rev. Lett. **20** (1968) 1127; Phys. Rev. **181** (1969) 2141; Phys. Rev. **D6** (1972) 3522.
- [61] M.G. Olsson, Ulf-G. Meißner, N. Kaiser and V. Bernard. “On the interpretation of the $\pi N \rightarrow \pi\pi N$ data near threshold”. Preprint CRN 95-13, MADPH-95-866, TK 95 07 (1995).
- [62] M.G. Olsson and E.T. Osypowski. Nucl. Phys. **B101** (1975) 136.
- [63] E. Oset and M.J. Vicente–Vacas. Nucl. Phys. A **446** (1985) 584.
- [64] W.A. Perkins, J.C. Caris, R.W. Kenney, V. Perez-Mendez. Phys. Rev., **118** (1960) 1364.
- [65] A. Pich. Rep. Prog. Phys. **58** (1995) 563.
- [66] D. Počanić, E. Frlež, K.A. Assamagan, et al. Phys. Rev. Lett. **72** (1994) 1156.
- [67] D. Počanić. In Proceedeng of Conference “Meson and Nuclei at Intermediate Energies”, May 3–7, 1994, Dubna. The Joint Institute for Nuclear Physics, Dubna, 1994.
- [68] D. Počanić. Summary of π – π Scattering Experiments, *in* A.M. Bernstein and B.R. Holstein (eds.), Chiral Dynamics: Theory and Experiment, Proceedings of the Workshop held at MIT, Cambridge, MA, USA, 25–29 July 1994, Lecture Notes in Physics, LNP 452 (Springer–Verlag, Berlin and Heidelberg, 1995), p. 95.
- [69] C. Rebbi. Ann. Phys. (NY) **49** (1968) 106.
- [70] Review of Particle Physics. Phys. Rev. **D54** (1996) Number 1.
- [71] D.H. Saxon, J.H. Mulvey, W. Chinowsky. Phys. Rev. **D2** (1970) 1790-1803.
- [72] M.E. Sevier, A. Ambardar, et al. Phys. Rev. Lett. **66** (1991) 2569-2572.

- [73] M.E. Sevier. Preliminary results of a new measurement of the reaction $\pi^+p \rightarrow \pi^+\pi^+n$ near threshold. *in* A.M. Bernstein and B.R. Holstein (eds.), Chiral Dynamics: Theory and Experiment, Proceedings of the Workshop held at MIT, Cambridge, MA, USA, 25–29 July 1994, Lecture Notes in Physics, LNP 452 (Springer–Verlag, Berlin and Heidelberg, 1995), p. 114.
- [74] G.R. Smith and M. Kermani, “Experiment 624: The $(\pi, 2\pi)$ reaction, a tool to determine scattering lengths and coupling constants”. TRIUMF Annual Report Scientific Activities 1994.
- [75] G.R. Smith, et al. Nucl. Instr. and Meth. **A362** (1995) 349.
- [76] D.I. Sober, M. Arman, et al. Phys. Rev. **D11** (1975) 1017-1035.
- [77] J. Stern, H. Sazdjian and N.H. Fuchs. Phys. Rev. **D47** (1993) 3814.
- [78] M. Svec. Phys. Rev. **D46** (1992) 949.
- [79] M. Svec. Phys. Rev. **D55** (1997) 4355.
- [80] V.V. Vereshagin, S.G. Sherman, et al. Nucl. Phys., **A592** (1995) 413.
- [81] S. Weinberg. Physica **96A** (1979) 327

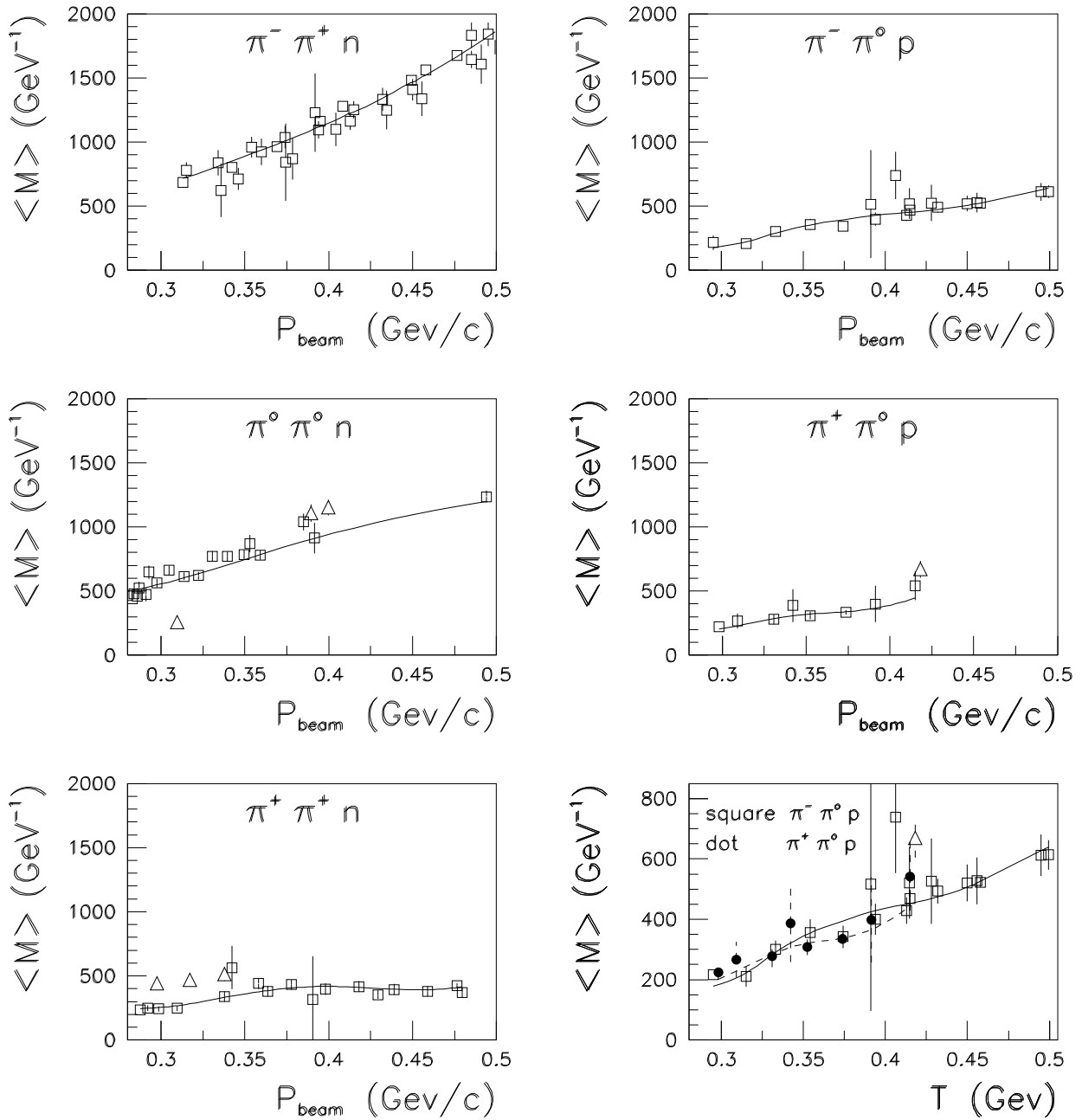


Figure 2: Experimental points of total cross sections and the theoretical curve for the best physical solution (quasi-amplitude $\langle M \rangle$ in GeV^{-1}). Triangle points were excluded from fittings.

Kirz ($P = 477 \text{ Mev}/c$)

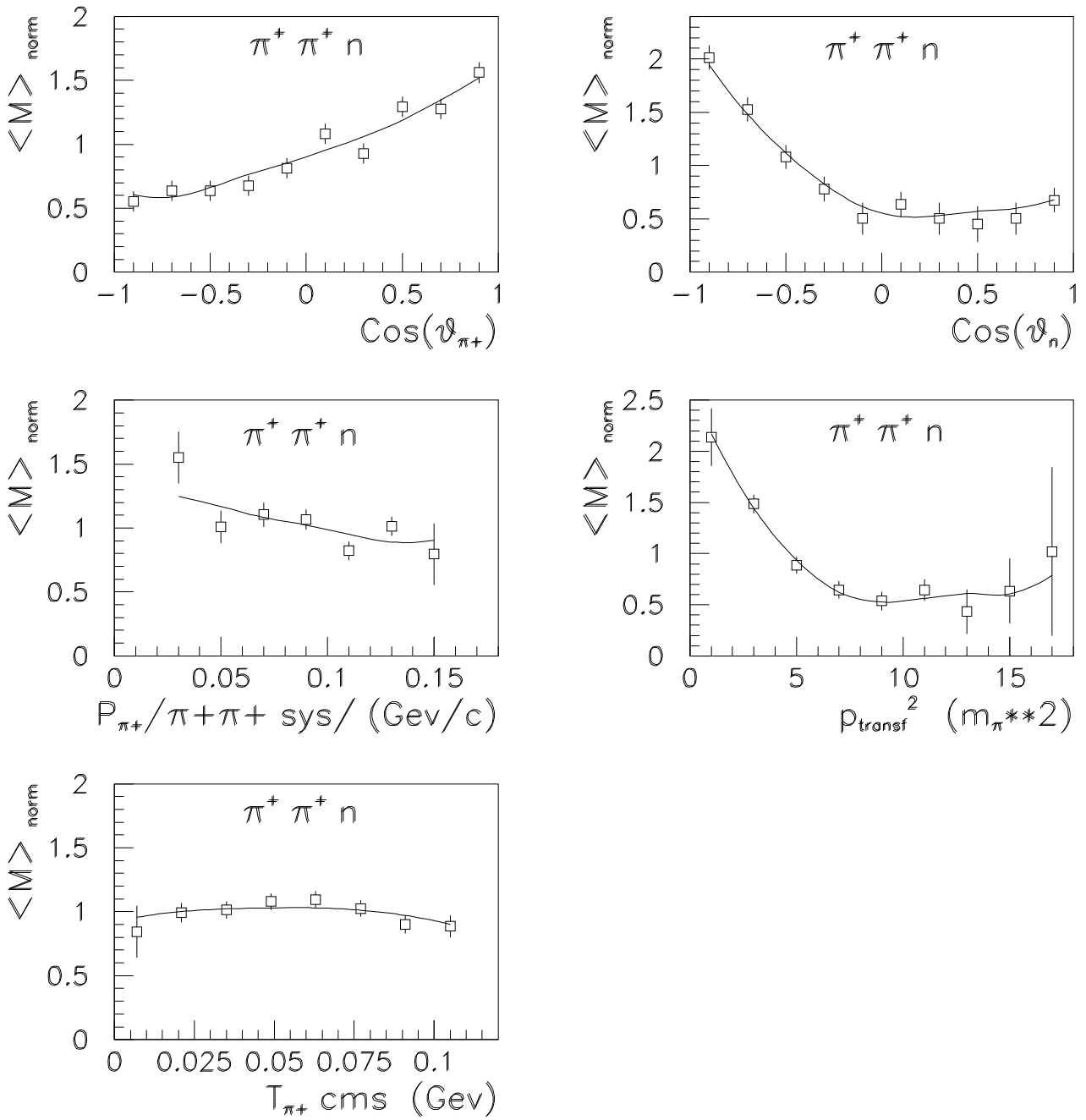


Figure 3: Experimental distributions for the $\{++n\}$ channel from the paper [45] by Kirz and theoretical curves (normalized quasi-amplitude $\langle M \rangle_{\text{norm}}$).

Jones (P=415 Mev/c)

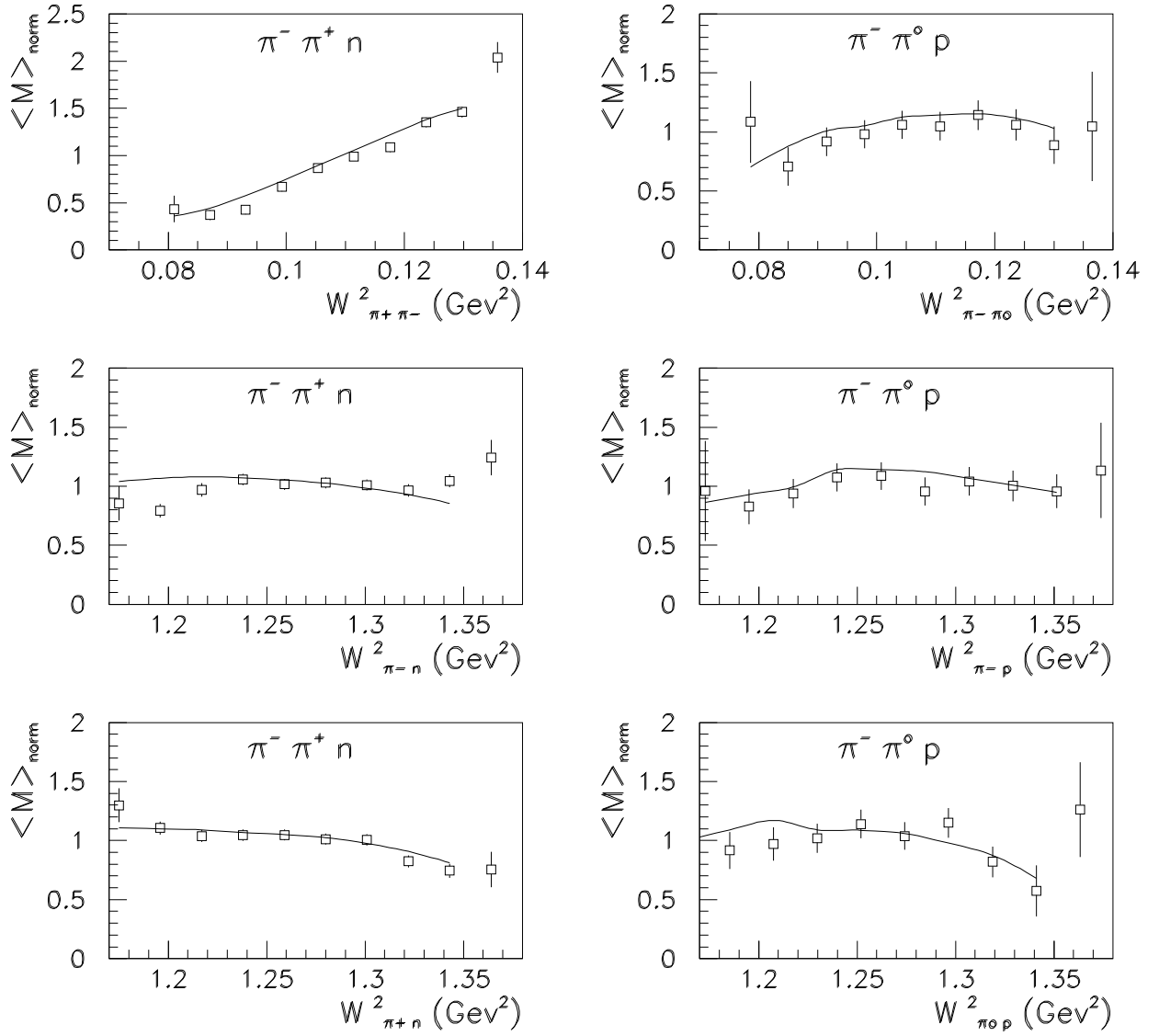


Figure 4: Experimental distributions for the $\{- + n\}$ and $\{- + n\}$ channels from the paper [38] by Jones and theoretical curves (normalized quasi-amplitude $\langle M \rangle_{\text{norm}}$).

Kirz (P = 485 Mev/c)

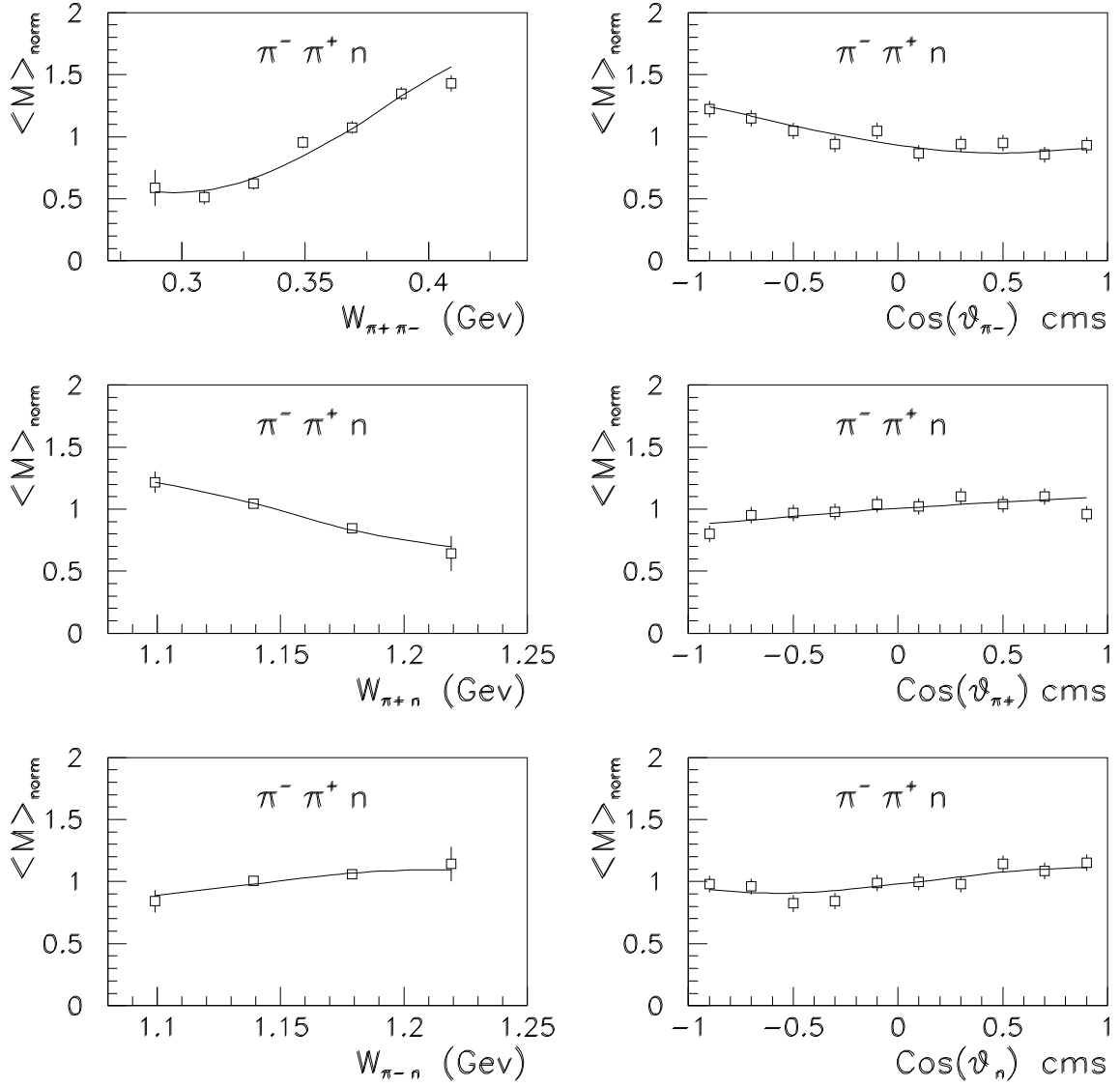


Figure 5: Experimental distributions for the $\{- + n\}$ channel from the paper [46] by Kirz and theoretical curves (normalized quasi-amplitude $\langle M \rangle_{\text{norm}}$).

Dubna ($P = 460 \text{ Mev}/c$)

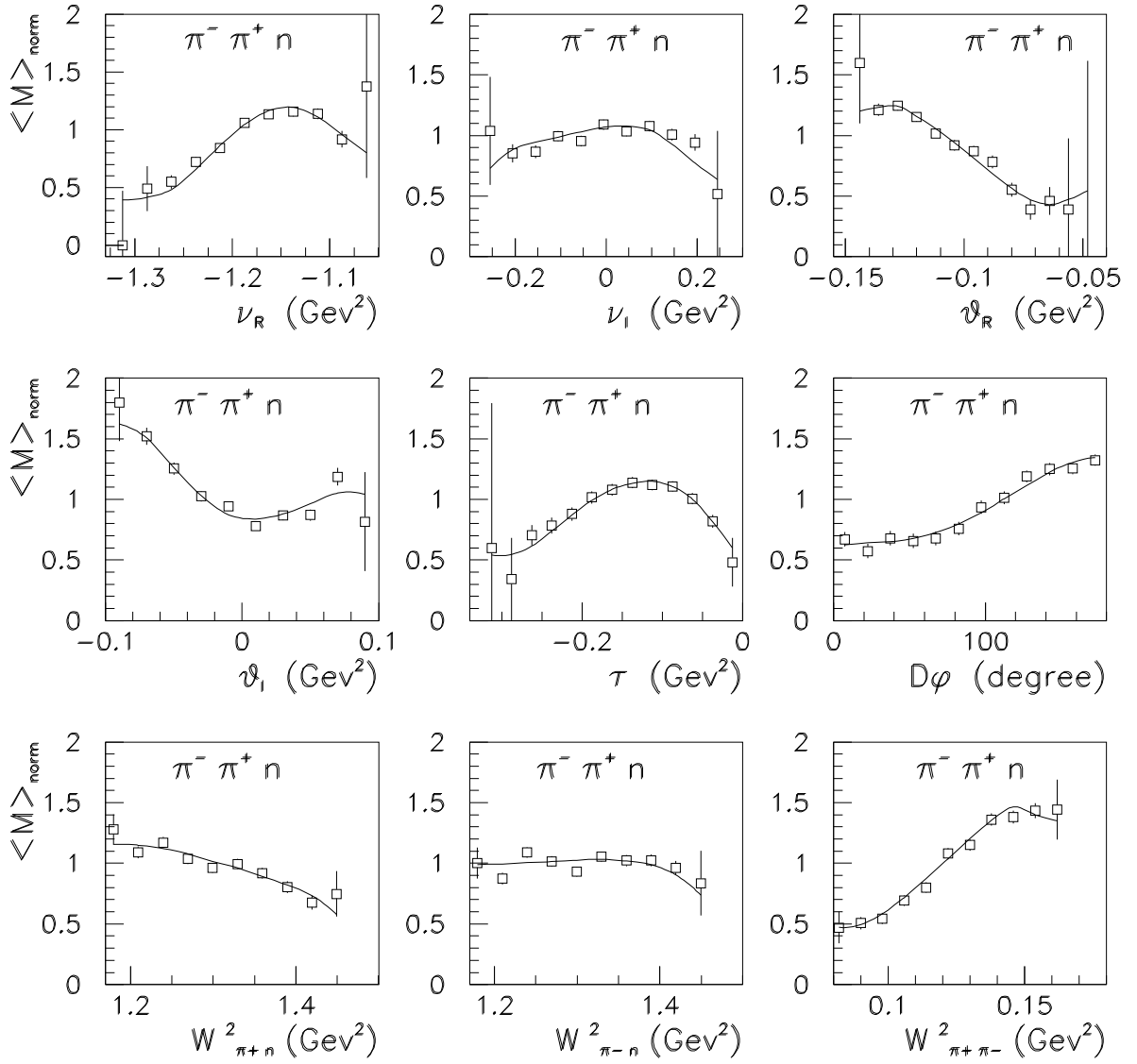


Figure 6: Some of experimental distributions for the $\{- + n\}$ channel from the paper [18] by Blokhintseva and theoretical curves (normalized quasi-amplitude $\langle M \rangle_{\text{norm}}$).

Dubna(P=460 Mev/c) Saxon(P=456 Mev/c) Saxon(P=505 Mev/c)

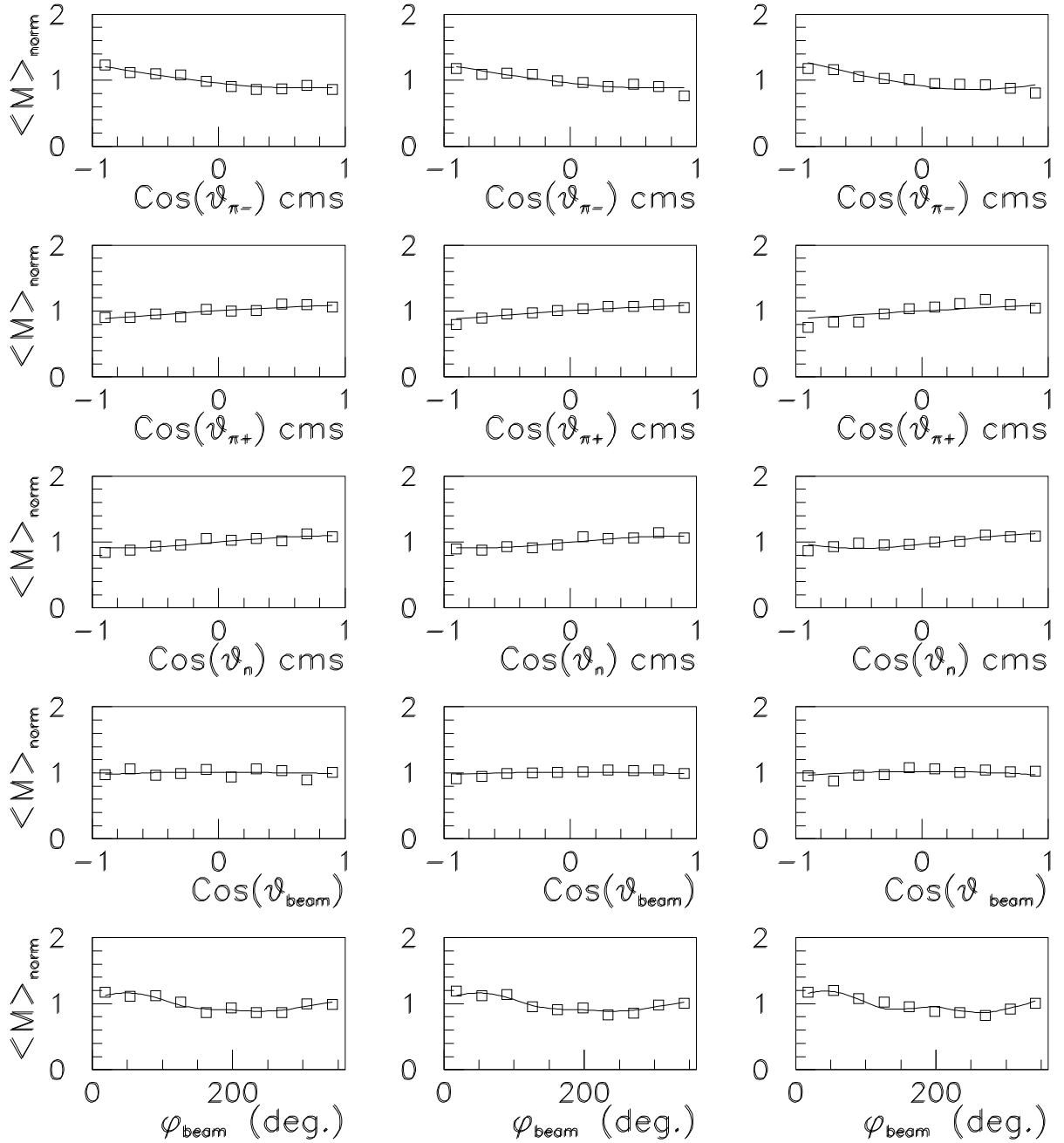


Figure 7: Experimental distributions and theoretical curves for angular spectra of the $\{- + n\}$ channel from the Saxon's paper [71] and the same spectra build of the Blokhintseva data [18] (normalized quasi-amplitude $\langle M \rangle_{\text{norm}}$). The Saxon data had not been used in fittings.

Saxon(P=456)

Saxon(P=505)

Kirz(P=557)

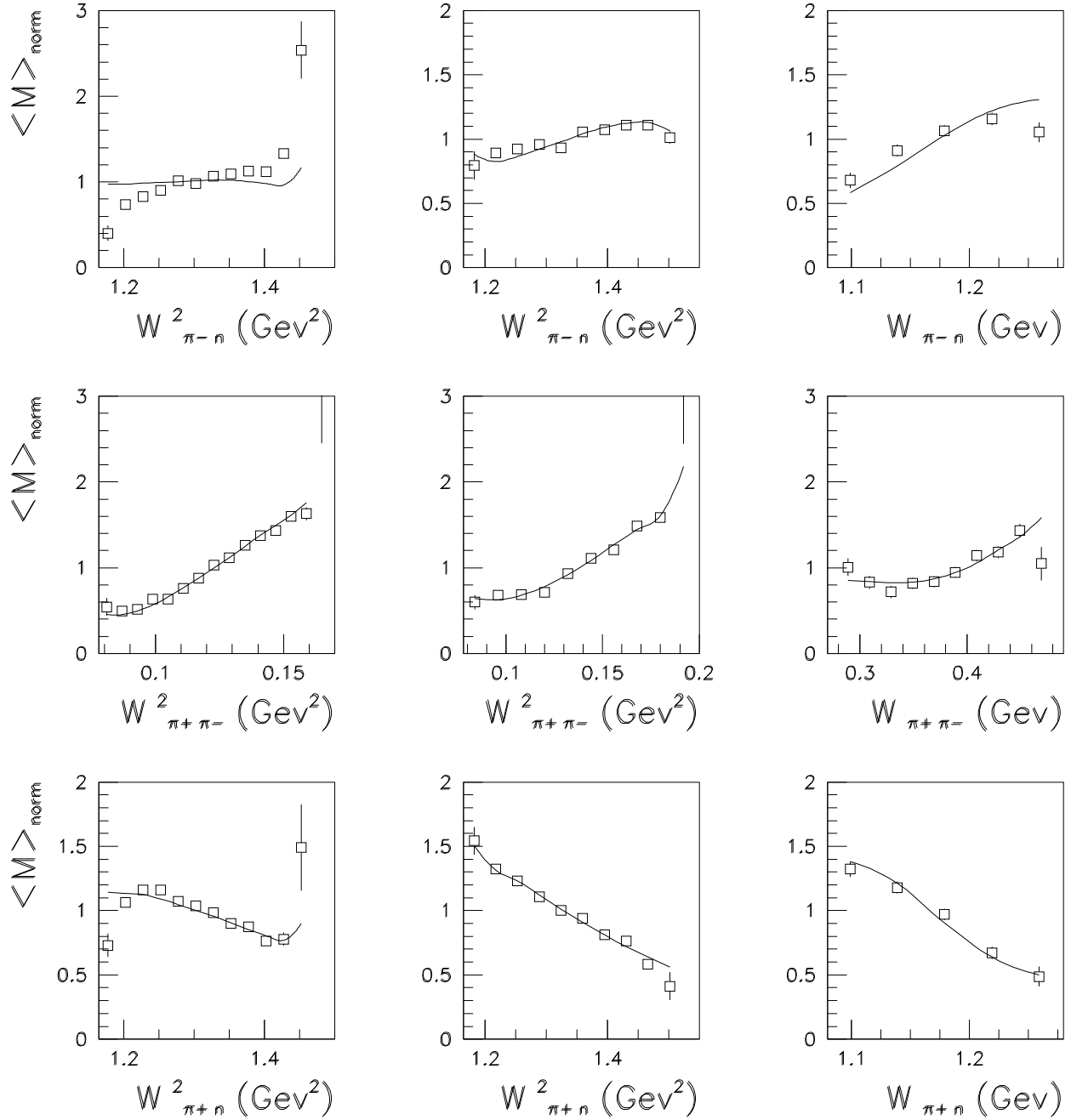


Figure 8: Experimental distributions and theoretical predictions for spectra of the $\{- + n\}$ channel from the paper [71] by Saxon and from the paper [46] by Kirz (normalized quasi-amplitude $\langle M \rangle_{\text{norm}}$).

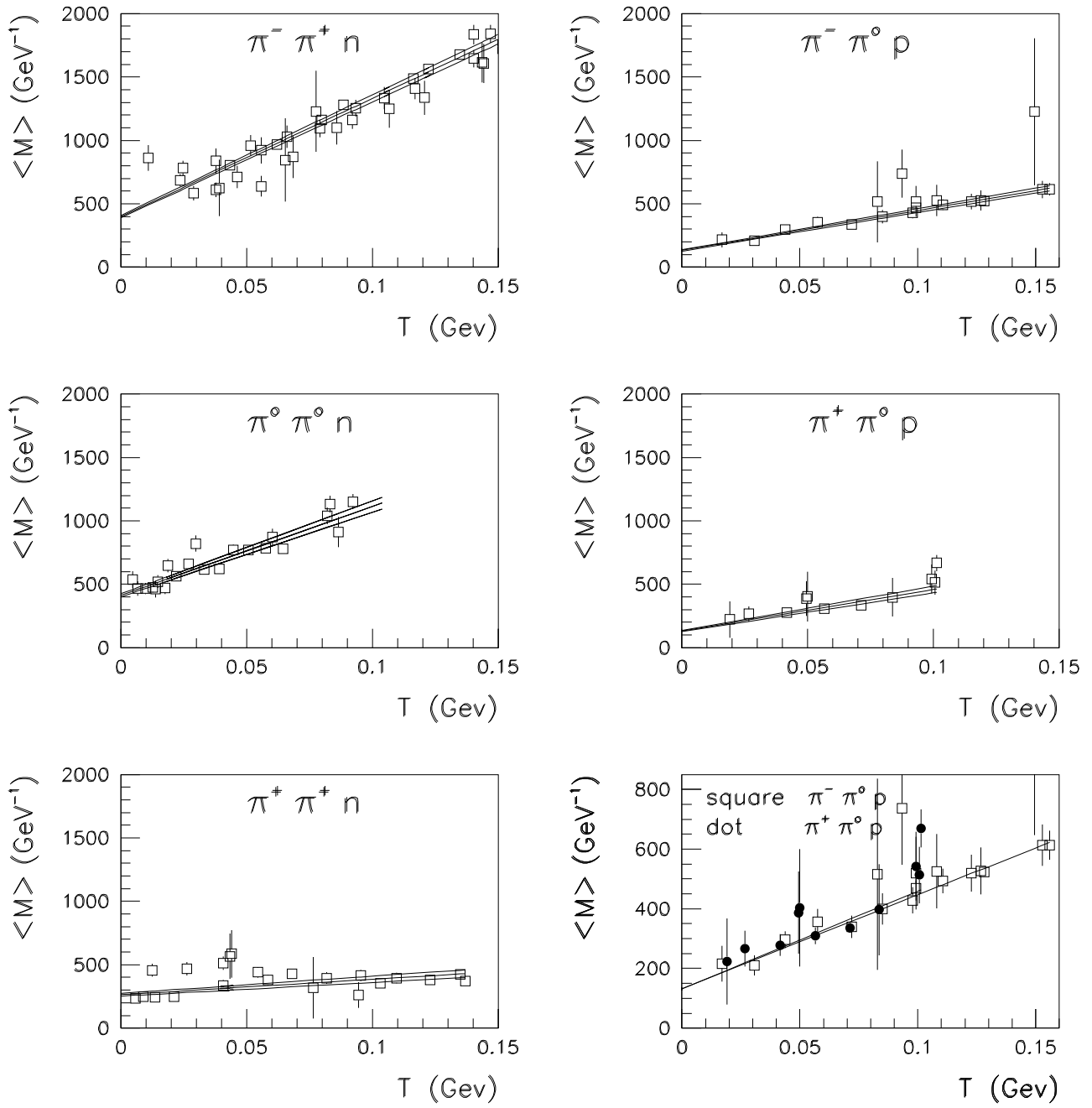


Figure 9: Linear fit of total cross sections of all five channels with 7 parameters (quasi-amplitude $\langle M \rangle$ in GeV^{-1}).

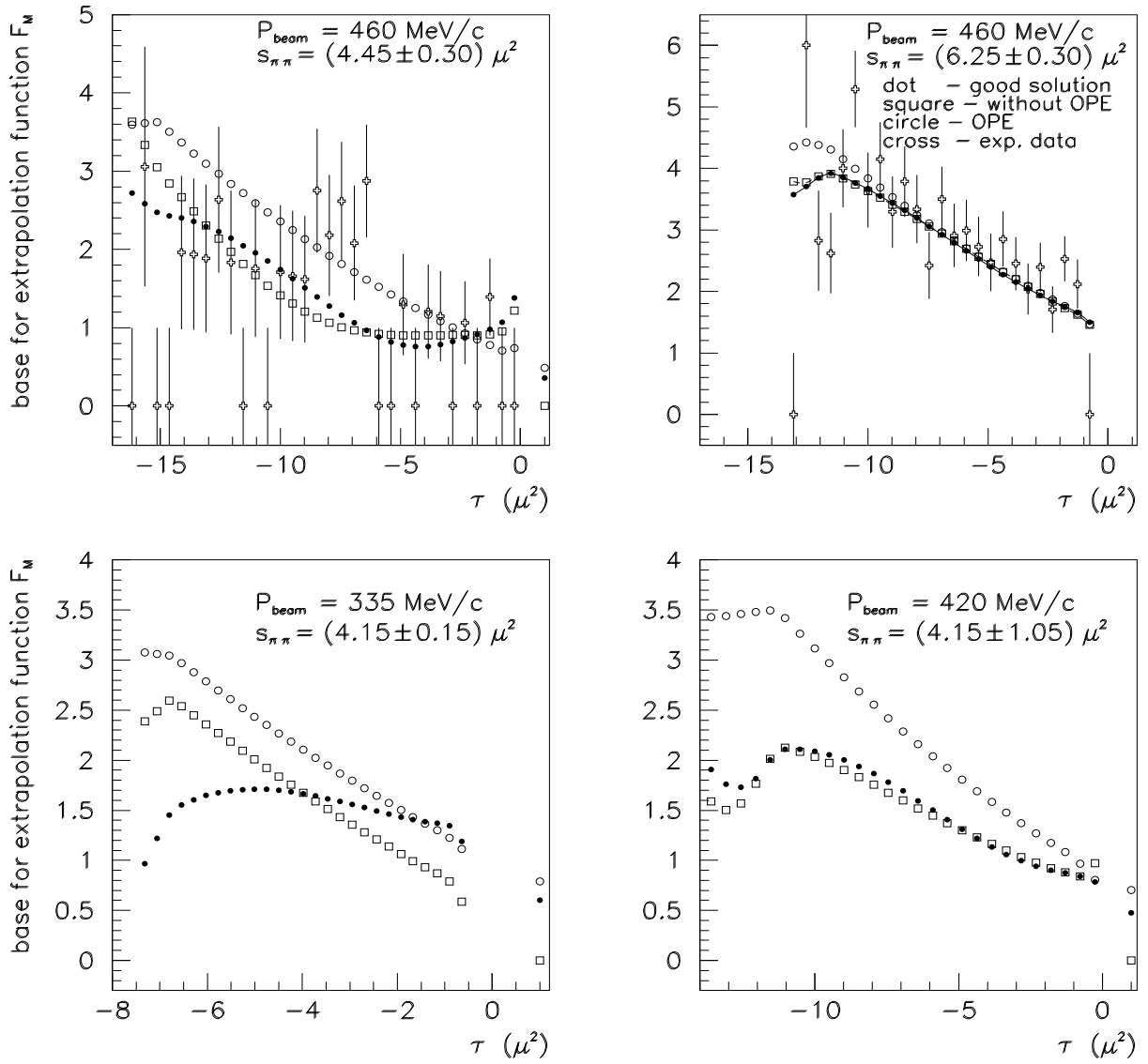


Figure 10: Simulations of extrapolation data (F_M): dot — the amplitude of the best physical solution; square — the amplitude without the OPE contribution; circle — the pure OPE amplitude; cross — the available experimental data of the paper [18] by Blokhintseva.